Age-Related Changes in D-Aspartate Oxidase Promoter Methylation Control Extracellular D-Aspartate Levels and Prevent Precocious, Cell Death during Brain Aging

This article shows the essential epigenetic control of D-Aspartate Oxidase (DDO), elucidating its role in preventing precocious cell death and brain aging by degrading the D-aminoacid Aspartate. I participated in the characterization of *DDO* expression pattern during development and post-natal life in the mouse brain by means radioactive *in situ* hybridization experiments. Moreover, I investigated the effect of persistent elevated D-Aspartate levels in DDO -/- mice, focusing of lipofuscin inclusion bodies by means of confocal miscroscopy and 3D analysis.

Neurobiology of Disease

Age-Related Changes in D-Aspartate Oxidase Promoter Methylation Control Extracellular D-Aspartate Levels and Prevent Precocious Cell Death during Brain Aging

Daniela Punzo,[1,2*] Francesco Errico,[3,4*] Luigia Cristino,[5*] Silvia Sacchi,[6,7] Simona Keller,[1,4] Carmela Belardo,[8] Livio Luongo,[8] Tommaso Nuzzo,[2,3] Roberta Imperatore,[5] Ermanno Florio,[1,4] Vito De Novellis,[8] Ornella Affinito,[1,4] Sara Migliarini,[9] Giacomo Maddaloni,[9] Maria Josè Sisalli,[1] Massimo Pasqualetti,[9,10] Loredano Pollegioni,[6,7] Sabatino Maione,[8] Lorenzo Chiariotti,[1,4] and Alessandro Usiello[2,3]

[1]Istituto di Endocrinologia ed Oncologia Sperimentale, Consiglio Nazionale delle Ricerche (CNR), 80131 Naples, Italy, [2]Department of Environmental, Biological and Pharmaceutical Sciences and Technologies, Second University of Naples, 81100 Caserta, Italy, [3]Laboratory of Behavioural Neuroscience, Ceinge Biotecnologie Avanzate, 80145 Naples, Italy, [4]Department of Molecular Medicine and Medical Biotechnology, University of Naples Federico II, 80131 Naples, Italy, [5]Institute of Biomolecular Chemistry, CNR, 80078 Pozzuoli, Italy, [6]Department of Biotechnology and Life Sciences, University of Insubria, 21100 Varese, Italy, [7]Protein Factory Research Center, Politecnico di Milano and University of Insubria, 20133 Milan, Italy, [8]Department of Experimental Medicine, Section of Pharmacology, Second University of Naples, 80138 Naples, Italy, [9]Department of Biology, Unit of Cell and Developmental Biology, University of Pisa, 56126 Pisa, Italy, and [10]Center for Neuroscience and Cognitive Systems, Istituto Italiano di Tecnologia, 38068 Rovereto, Italy

The endogenous NMDA receptor (NMDAR) agonist D-aspartate occurs transiently in the mammalian brain because it is abundant during embryonic and perinatal phases before drastically decreasing during adulthood. It is well established that postnatal reduction of cerebral D-aspartate levels is due to the concomitant onset of D-aspartate oxidase (DDO) activity, a flavoenzyme that selectively degrades bicarboxylic D-amino acids. In the present work, we show that D-aspartate content in the mouse brain drastically decreases after birth, whereas *Ddo* mRNA levels concomitantly increase. Interestingly, postnatal *Ddo* gene expression is paralleled by progressive demethylation within its putative promoter region. Consistent with an epigenetic control on *Ddo* expression, treatment with the DNA-demethylating agent, azacitidine, causes increased mRNA levels in embryonic cortical neurons. To indirectly evaluate the effect of a putative persistent *Ddo* gene hypermethylation in the brain, we used *Ddo* knock-out mice ($Ddo^{-/-}$), which show constitutively suppressed *Ddo* expression. In these mice, we found for the first time substantially increased extracellular content of D-aspartate in the brain. In line with detrimental effects produced by NMDAR overstimulation, persistent elevation of D-aspartate levels in $Ddo^{-/-}$ brains is associated with appearance of dystrophic microglia, precocious caspase-3 activation, and cell death in cortical pyramidal neurons and dopaminergic neurons of the substantia nigra pars compacta. This evidence, along with the early accumulation of lipofuscin granules in $Ddo^{-/-}$ brains, highlights an unexpected importance of *Ddo* demethylation in preventing neurodegenerative processes produced by nonphysiological extracellular levels of free D-aspartate.

Key words: aging; D-amino acids; DNA methylation; neurodegeneration; NMDA receptor

Significance Statement

The enzyme D-aspartate oxidase (DDO) catalyzes the degradation of the NMDA receptor agonist, D-aspartate. In the brain, DDO is expressed only during postnatal life, thus reducing the embryonic storage of D-aspartate and keeping this D-amino acid at low levels during adulthood. Although the presence of DDO in mammals is long established, its biological role in the brain and the mechanism regulating its expression are still unclear. Here, we found that *Ddo* promoter demethylation enables the postnatal expression of *Ddo*. Moreover, persistent suppression of *Ddo* expression leads to persistent spillover of extracellular D-aspartate and produces precocious cell death in the mouse brain, thus suggesting a key role for DDO in preventing early neurodegeneration triggered by excessive NMDA receptor stimulation.

Introduction

Since the first discovery by Sir Hans Krebs in 1935, the presence of flavoproteins responsible for D-amino acids' deamination (Krebs, 1935; Still and Buell, 1949) is well known in mammals. In particular, D-aspartate oxidase (DDO or DASPO, EC 1.4.3.1) is a FAD-containing enzyme that selectively deaminates bicarboxylic D-amino acids, such as D-aspartate (D-Asp), NMDA, and D-glutamate (Still and Buell, 1949; Van Veldhoven et al., 1991; D'Aniello et al., 1993). DDO is expressed in both humans and rats (Van Veldhoven et al., 1991; Schell et al., 1997; Zaar et al., 2002). In the rat brain, DDO activity is nearly absent during embryonic and perinatal stages and progressively increases during adulthood (Van Veldhoven et al., 1991). Accordingly, free D-Asp (DDO endogenous substrate) shows a reciprocal temporal occurrence because it is substantially enriched in the embryonic brain, rapidly declines after birth, and remains at low levels throughout the adulthood (Dunlop et al., 1986; Neidle and Dunlop, 1990; Hashimoto et al., 1993, 1995; Sakai et al., 1998; Wolosker et al., 2000). Notably, in homogenates from human fetal prefrontal cortex (PFC), the amount of free D-Asp even exceeds that of the L-aspartate (L-Asp) at gestational week 14, before substantially decreasing at postnatal stages (Hashimoto et al., 1993). The peculiar temporal pattern of DDO expression in the rat brain suggests that this catabolic enzyme acts to maintain low levels of D-Asp during postnatal brain development. However, the biological meaning of the prominent postnatal DDO activity is still unclear. Likewise, it is still unknown whether abundant free D-Asp levels play any physiological role during embryonic and perinatal brain development. Recent evidence from mouse brain tissue slices has shown that free D-Asp activates the NMDA receptors (NMDARs) via binding to the GluN2 subunit (Errico et al., 2008a, b; 2011a, b). In this line, studies performed in mice lacking the *Ddo* gene ($Ddo^{-/-}$) and in chronically D-Asp-treated mice have demonstrated that the resulting increase in free D-Asp in the brain (Errico et al., 2006; Huang et al., 2006) affects NMDAR-dependent transmission (Errico et al., 2008a, b, 2011a, b, 2014; Krashia et al., 2015), early- and late-phase hippocampal LTP (Errico et al., 2008b, 2014), dendritic length and spine density of hippocampal and cortical neurons (Errico et al., 2014), and spatial memory abilities (Errico et al., 2008a, 2011a, b). Furthermore, higher levels of D-Asp in $Ddo^{-/-}$ mice are also associated with greater brain connectivity, as well as reduced sensorimotor gating deficits and abnormal circuits activation induced by the hallucinogenic drug, phencyclidine, as assessed by fMRI (Errico et al., 2015b). Consistent with these findings in mice, a human *DDO* gene variant (rs3757351), yielding reduced expression levels of *DDO* mRNA in postmortem prefrontal cortex, is associated with both greater prefrontal gray matter and activity (fMRI) during working memory processing in healthy subjects (Errico et al., 2014).

Based on the basic and translational interest of free D-amino acids in brain physiology and in the treatment of psychiatric disorders, such as schizophrenia (Tsai et al., 1998, 2006; Heresco-Levy et al., 2005; Lane et al., 2005; Kantrowitz et al., 2010), we aim here to do the following: (1) elucidate the molecular mechanism regulating the postnatal cerebral expression of DDO; (2) investigate how the targeted deletion of *Ddo* affects extracellular levels of free D-Asp in the brain; and (3) clarify the physiological relevance of this enzyme in the mammalian brain during aging.

Materials and Methods

Animals. All experiments were performed on male animals. C57BL/6J mice were purchased from The Jackson Laboratory. Knock-out mice for the *Ddo* gene were generated and genotyped by PCR as described previously (Errico et al., 2006). Wild-type ($Ddo^{+/+}$) and knock-out ($Ddo^{-/-}$) mice, derived from mating of heterozygous ($Ddo^{+/-}$) mice, were backcrossed to the F5 generation to C57BL/6J strain. Mice were housed in groups ($n = 4$ or 5) in standard cages (29 × 17.5 × 12.5 cm) at constant temperature (22 ± 1°C) and maintained on a 12/12 h light/dark cycle, with food and water *ad libitum*. All research involving animals was performed in accordance with the European directive 86/609/EEC governing animal welfare and protection, which is acknowledged by the Italian Legislative Decree no. 116 (January 27, 1992). Animal research protocols were also reviewed and consented to by a local animal care committee. All efforts were made to minimize the animal's suffering.

Mouse tissue collection. Whole brains were collected from C57BL/6J mice at different developmental stages, including the following time points: embryonic day 15 (E15; $n = 5$), postnatal day 0 (P0; $n = 2$), P7 ($n = 3$), P14 ($n = 6$), P21 ($n = 3$), P30 ($n = 3$), and P60 ($n = 3$). The PFC and ventral midbrain were dissected out from 3-month-old $Ddo^{+/+}$ and $Ddo^{-/-}$ mice (PFC, $n = 5$/genotype; midbrain, $n = 4$/genotype). Mice were killed, and the whole brain, PFC, or midbrain was dissected out within 20 s on an ice-cold surface. All tissue samples were pulverized in liquid nitrogen and stored at −80°C for subsequent processing.

HPLC analyses. Brain tissue samples were analyzed as previously reported (Topo et al., 2010), with minor modifications. They were homogenized in 1:20 (w/v) 0.2 M TCA, sonicated (3 cycles, 10 s each), and centrifuged at 10,000 × *g* for 10 min. The precipitated protein pellets were stored at −80°C for protein quantification, whereas the supernatants were neutralized with NaOH and subjected to precolumn derivatization with o-phthaldialdehyde (OPA)/*N*-acetyl-L-cysteine in 50% methanol. Enantiomer derivatives were then resolved on a Simmetry C8 5 μm reversed-phase column (Waters, 4.6 × 250 mm), in isocratic conditions (0.1 M sodium acetate buffer, pH 6.2, 1% tetrahydrofuran, 1 ml/min flow rate). A washing step in 0.1 M sodium acetate buffer, 3% tetrahydrofuran and 47% acetonitrile, was performed after every single run. Identification and quantification of D-and L-Asp was based on retention times and peak areas, compared with those associated with external standards. The two enantiomers were detected as well-defined peaks at the retention time of 4.75 ± 0.1 min and 5.33 ± 0.1 min for D-and L-Asp, respectively (see Fig. 1*a*,*b*). The identity of D-Asp and L-Asp peaks was confirmed either by the selective degradation catalyzed by the *RgDAAO* M213R variant (Sacchi et al., 2002) (see Fig. 1*a*, inset) and *StLASPO* (Bifulco et al., 2013), respectively, or by the addition of external standards (see Fig. 1*b*, inset). The samples were added with 10 μg of the enzymes, incubated at 30°C for 30 min, and then derivatized (Topo et al., 2010). Total protein content of homogenates was determined using the Bradford assay method after resolubilization of the TCA precipitated protein pellets. The detected total concentration of D-Asp and L-Asp in homogenates was normalized by the total protein content. Data on the ontogenetic occurrence of D-and L-Asp in the whole brain were analyzed by one-way ANOVA (age effect); data on D-and L-Asp occurrence in the

Received Oct. 27, 2015; revised Jan. 5, 2016; accepted Jan. 23, 2016.

Author contributions: F.E. and A.U. designed research; D.P., L. Cristino, S.S., S.K., C.B., L.L., T.N., R.I., E.F., O.A., S. Migliarini, G.M., and M.J.S. performed research; V.D.N., M.P., L.P., S. Maione, and L. Chiariotti analyzed data; F.E. and A.U. wrote the paper.

A.U. was supported by 2013 National Alliance for Research on Schizophrenia and Depression Independent Investigator Grant 20353 from the Brain and Behavior Research Foundation. F.E. was supported by 2015 National Alliance for Research on Schizophrenia and Depression Young Investigator Grant 23968 from the Brain and Behavior Research Foundation, and the Italian Ministry of Education, Universities and Research (FIRB Call-Program Futuro in Ricerca 2010, Project RBFR10XCD3). S.S. and L.P. were supported by Fondo di Ateneo per la Ricerca. L. Chiariotti was supported by Epigenomics Flagship Project (CNR). We thank Wolfgang Kelsch, Francisco Zafra, and Darrick Balu for critical discussion; and Marta Squillace, Giuseppe Aceto, and Anna Di Maio for technical support.

The authors declare no competing financial interests.

*D.P., F.E., and L. Cristino contributed equally to this study as co-first authors.

Correspondence should be addressed to either of the following: Dr. Lorenzo Chiariotti, Department of Molecular Medicine and Medical Biotechnology, University of Naples Federico II, Via Pansini 5, 80131 Naples, Italy, E-mail: chiariot@unina.it; or Dr. Alessandro Usiello, Ceinge Biotecnologie Avanzate, Via G. Salvatore 486, 80145 Naples, Italy, E-mail: usiello@ceinge.unina.it.

DOI:10.1523/JNEUROSCI.3881-15.2016

PFC and midbrain of *Ddo*$^{+/+}$ and *Ddo*$^{-/-}$ mice were analyzed by Student's *t* test (genotype effect).

Dialysates were analyzed for D-Asp, L-Asp, and L-Glu content, as previously described (Guida et al., 2015). The HPLC system comprised a Varian ternary pump (model 9010), a C18 reverse-phase column, a Varian refrigerated autoinjector (model 9100), and a Varian fluorimetric detector. Dialysates were precolumn derivatized with OPA (10 μl dialysate + 10 μl OPA) and amino acid conjugates resolved using a gradient separation. The mobile phase consisted of the following two components: (1) 0.2 M sodium phosphate buffer, pH 5.8, 0.1 M citric acid, pH 5.8; and (2) 90% acetonitrile. The identity of D-Asp peak was confirmed by incubating a parallel sample with 20 μg of purified DDO (Negri et al., 1999) for 15 min at 37°C and chromatographed as above. Identification and quantification of D-and L-Asp, as well as L-Glu, were performed as reported above. Data were collected by a Dell PC system 310 interfaced by Varian Star 6.2 control data and acquisition software. Amino acid extracellular levels were expressed as nM (D-Asp and L-Asp) or μM (L-Glu) concentration. Data were analyzed by two-way ANOVA with repeated measures (genotype × time).

Enzymes. Recombinant *Rhodotorula gracilis* D-amino acid oxidase M213R variant (*RgDAAO* M213R; EC 1.4.3.3) and *Sulfolobus tokodaii* L-aspartate oxidase (*StLASPO*; EC 1.4.3.16) were overexpressed in *Escherichia coli* cells and purified as previously described (Sacchi et al., 2002; Bifulco et al., 2013). Final *RgDAAO* M213R and *StLASPO* preparations had a specific activity of 5.8 U/mg protein on D-Asp as substrate and 0.98 U/mg protein on L-Asp as substrate, respectively, whereas they were fully inactive on the opposite enantiomers. Recombinant DDO (EC 1.4.3.1) from beef kidney was expressed in *E. coli*, and the purified preparation showed a specific activity of 5 U/mg protein (Negri et al., 1999).

In vivo *microdialysis.* Microdialysis experiments were performed in awake and freely moving mice as previously reported (Guida et al., 2015). Three-month-old *Ddo*$^{+/+}$ and *Ddo*$^{-/-}$ mice were anesthetized with pentobarbital (50 mg/kg, i.p.), and the concentric microdialysis probes were stereotaxically implanted into the PFC area (anteroposterior: 1.5 mm; L: 0.3; and ventral: 3.3 mm below the dura) and secured to the skull using stainless steel screws and dental cement. Microdialysis probes were constructed with 22G (0.41 mm I.D., 0.7 mm O.D.) stainless steel tubing: inlet and outlet cannulae (0.04 mm I.D., 0.14 mm O.D.) consisted of fused silica tubing. The probe had a tubular dialysis membrane (Enka) 1.3 mm in length. After a postoperative recovery period of ~48 h, dialysis was commenced with ACSF (147 mM NaCl, 2.2 mM $CaCl_2$, 4 mM KCl, pH 7.2). Animals were perfused at a rate of 1.2 μl/min using a Harvard Apparatus infusion pump (model 22). After an equilibration period of 60 min, samples were collected every 30 min for a total time length of 180 min. The last dialysate fraction (150–180 min) was collected in the absence of calcium by perfusing with Ca^{2+}-free ACSF solution. Dialysates were analyzed for D-Asp, L-Asp, and L-Glu content using HPLC coupled with the fluorimetric detection method.

In situ *hybridization (ISH).* ISH analysis was performed on sagittal sections from E15, P0, P14, P30, and P60 C57BL/6J brains (n = 3 per age), *Ddo*$^{+/+}$ or *Ddo*$^{-/-}$ brains (n = 3 per genotype) according to a protocol previously described (Migliarini et al., 2013). ^{35}S-labeled *Ddo* antisense riboprobes (1.9 kb) were used. Hybridized sections were exposed to Biomax MR x-ray films (Kodak) for 7–9 d. Sections were examined using brightfield light microscopy. To obtain clearer and more defined images, less disturbed by the background noise, pseudocolor scale of the images was used. Signals were pseudocolored with the National Institutes of Health ImageJ Lookup Table 16_colors.

RNA extraction and qRT-PCR. Total RNA was extracted by TRIZOL reagents (Ambion, Invitrogen) according to the manufacturer's instructions. The integrity of the RNA was assessed by denaturing agarose gel electrophoresis (presence of sharp 28S, 18S, and 5S bands) and spectrophotometry (NanoDrop 2000, Thermo Scientific). Total RNA was purified to eliminate potentially contaminating genomic DNA using recombinant DNase (QIAGEN). A total of 1 μg of total RNA of each sample was reverse-transcribed with QuantiTect Reverse Transcription (QIAGEN) using oligo-dT and random primers according to the manufacturer's instructions. qRT-PCR amplifications were performed using LightCycler 480 SYBR Green I Master (Roche Diagnostic) in a LightCycler 480 Real Time thermocycler (Roche). The following protocol was used: 10 s for initial denaturation at 95°C followed by 40 cycles consisting of 10 s at 94°C for denaturation, 10 s at 60°C for annealing, and 6 s for elongation at 72°C temperature. The following primers were used for mouse *Ddo* cDNA amplification: *Ddo* forward 5′-ACCACCAGTAATG TAGCGGC3′ and *Ddo* reverse 5′-GGTACCGGGGTATCTGCAC-3′; β-actin gene was used as housekeeping gene forPCR: β-actin forward 5′-CT AAGGCCAACCGTGAAAAG-3′ and β-actin reverse 5′-ACCAG AGGCATACAGGGACA-3′. Data were analyzed by one-way ANOVA (age effect).

5-Aza-2′-deoxycytidine treatment of primary cortical neurons. Cortical neurons were prepared from brains of 17-day-old C57BL/6J mouse embryos as previously described (Sisalli et al., 2014). Briefly, the mice were first anesthetized and then killed by cervical dislocation to minimize the animals' pain and distress. Dissection and dissociation were performed in Ca^{2+}/Mg^{2+}-free buffer saline (HBSS 1×). Tissues were incubated with trypsin for 20 min at 37°C and dissociated by trituration in culture medium. Cells were plated at 3.5–5 × 10^6 in 60 mm plastic Petri dishes, precoated with poly-D-lysine (20 mg/ml), in MEM/F12 (Invitrogen)-containing glucose, 5% deactivated FBS, and 5% horse serum (Invitrogen), glutamine, and antibiotics. Ara-C (10 mM) was added within 48 h of plating to prevent non-neuronal cell growth. Neurons were cultured at 37°C in a humidified 5% CO_2 atmosphere. Forty-eight hours of treatment of neuronal cultures was done with 5-aza-2′-deoxycytidine at a final concentration of 5 μM (Sigma-Aldrich). All the experiments on primary cortical neurons were performed according to the procedures described in experimental protocols approved by the Ethical Committee of the Federico II University of Naples. RNA extraction and qRT-PCR were performed as described above.

DNA extraction and methylation analysis. DNA from frozen brain tissue samples was extracted using the ZR Genomic DNA tissue Midi Prep kit (Zymo Research). The integrity and the amount of genomic DNA were assessed by 0.8% agarose gel electrophoresis and Qubit Fluorometric Quantitation (Invitrogen). Sodium bisulfite conversion was performed using EZ DNA Methylation Kit (Zymo Research). A total of 2 μg of genomic DNA was used according to the manufacturer's instruction. Methylation status was assessed through a strategy based on the locus-specific amplification of bisulfite-treated genomic DNA, amplifying each amplicon separately, followed by Illumina MiSeq sequencing. Fusion primers were designed to generate tiled amplicons ranging in size between 400 and 500 bp segments. Sequence of the bisulfite-specific primers used for this analysis were as follows: *Ddo* PR1 forward 5′-gtgtgtttTtgaggaggtgaTaTtTa-3′ (nt position from −468 to −444) and *Ddo* PR1 reverse 5′-aActtaccctccattAAtccatAcc-3′ (nt −88 to −63) for the *Ddo* promoter region 1 (amplicon size 405 bp) and *Ddo* PR2 forward 5′-ggTtggtggTaagTtgaagttTttg-3′ (nt −229 to −204) and *Ddo* PR2 reverse 5′-acccctaaaatcccaAaAtAcatac-3′ (nt 118 to 143) for the *Ddo* promoter region 2 (amplicon size 372). The capital letters in the primers sequences indicate the original C or G, respectively. The methods involved two PCR steps, following Illumina recommended procedure. The pool of amplicons was subjected to sequencing using MiSeq system (V3 reagents kits). Sequencing was performed by 281 × 2 cycles (paired-end sequencing). Sequences in FASTQ format by Illumina sequencing machine were initially processed with Paired-End reAd mergeR (PEAR) data for an initial quality filtering and assembling (R1 plus R2). Only those sequences with a threshold quality score of ≥30, a read length between 400 and 500 nt, and an overlapping region within paired-end reads of 40 nt were processed with PReprocessing and INformation of SEQuence (Prinseq) to obtain FASTA for further analysis. On average, ~232,000 (range: 139,241–368,083) amplicon reads were obtained from each sample. Reads were aligned to the bisulfite converted reference sequence. Methylation states were estimated by observing base calls (T/C) at CpG sites in the mapped reads. Reads with ambiguous calls at the CpG dinucleotide were removed. After filtering, an average of ~200,000 (range: 119,040–317,832) amplicon reads were obtained from each sample. Data were analyzed by one-way ANOVA (age effect).

Immunohistochemistry. Ddo$^{+/+}$ and *Ddo*$^{-/-}$ mice at 0.5, 3, 6, 10, and 13 months of age (n = 3 per genotype and age) were deeply anesthetized and transcardially perfused with a saline solution followed by 4% PFA in

0.1 M phosphate buffer. Morphological investigation of microglia was performed by incubation of sections with rabbit anti-Iba-1 primary antibody (1:1000 anti-ionized calcium-binding adapter molecule 1; Wako Chemicals) and revealed by appropriate secondary antibody (goat anti-rabbit, IgG-conjugated AlexaFluor-488; 1:1000; Invitrogen). The analysis of microglia was performed as previously described (Cristino et al., 2015). Briefly, quantitative analysis was performed by counting, for each phenotype, the bisbenzimide-counterstained cells with nucleus on the focal plane within a box measuring $2 \times 10^4\ \mu m^2$ in the substantia nigra pars compacta (SN). Resting microglia displayed small somata bearing long, thin, ramified processes. Activated microglia exhibited marked cellular hypertrophy and retraction of processes such that the process length was less than the diameter of the soma compartment. Dystrophic microglia was recognized by debris consisting of cells displaying fragmented processes as previously demonstrated in humans (Streit et al., 2009, 2014).

Moreover, serial 10 μm PFC and SN frozen sections were collected onto glass slides (Menzel) to be processed for Neuronal Nuclear (NeuN) marker immunoperoxidase (PFC) and for activated caspase-3/NeuN (PFC), or activated caspase-3/tyrosine hydroxylase (TH) (SN) immunofluorescence counterstained with DAPI. For NeuN immunoperoxidase staining, the PFC sections were reacted for 10 min in 0.1% H_2O_2 to inactivate endogenous peroxidase activity and then incubated with 10% normal goat serum (Vector Laboratories) in 0.1 M Tris-buffered saline, pH 7.6, containing 0.3% Triton X-100 and 0.05% sodium azide (Sigma). The sections were then incubated overnight at 4°C with normal goat serum diluted (range 1:200–1:400) rabbit polyclonal anti-NeuN (Abcam). After several rinses, the sections were incubated at room temperature for 2 h in biotinylated goat anti-rabbit IgGs (Vector Laboratories) followed 1 h by incubation in the avidin-biotin complex (ABC Kit; Vectastain, Vector) diluted in Tris-buffered saline according to the manufacturer's indications and then in 0.05% DAB for 10 min (DAB Sigma Fast, Sigma-Aldrich). Immunohistochemical study of activated caspase-3 in PFC and SN was performed by incubation with goat anti-activated caspase-3 (Santa Cruz Biotechnology) revealed by specific Alexa-488 secondary donkey anti-IgG antibody (Invitrogen) counterstained with DAPI. For activated caspase-3/NeuN or caspase-3/TH immunofluorescence, the sections were incubated with a mixture of goat anti-active caspase-3 (Santa Cruz Biotechnology) with rabbit polyclonal anti-NeuN (Abcam) or mouse anti-TH (Abcam) and revealed by a mixture of Alexa-488 and Alexa-546 secondary donkey anti-IgG antibodies (Invitrogen). TUNEL assay was performed on $n = 3$ sections (each from the rostral, medial, and caudal level of PFC or SN to be representative of the entire region) by using a commercial kit (Merck, Millipore) in accordance with the manufacturer's instructions. Caspase-3 and TUNEL assay were analyzed by Leica DMI6000 microscope equipped with appropriate filters and deconvolution MetaMorph LAS AF 2.2.0 software (Leica). Quantitative analysis was performed by counting the activated caspase-3-positive cells in $6.25 \times 10^4\ \mu m^2$ of PFC area/section ($n = 3$ sections per animal) and activated caspase-3/TH-positive neurons on $n = 200 \pm 20$ randomly selected TH-immunoreactive neurons ($n = 4$ SN sections per each genotype and age). Furthermore, activated caspase-3/NeuN-positive neurons were counted on $n = 200 \pm 20$ NeuN-immunoreactive neurons randomly selected ($n = 3$ PFC sections per genotype of 13 month-old mice). Statistical analysis was performed by two-way ANOVA (genotype × age), followed by Fisher's *post hoc* analysis between genotypes, when required.

Lipofuscin quantification. Sagittal 100-μm-thick Vibratome-cut sections obtained from $Ddo^{+/+}$ and $Ddo^{-/-}$ PFA-fixed brains at 0.5 and 3 months of age ($n = 3$ per genotype and age) were used. Free-floating sections were incubated with mouse anti-TH and subsequently with an Oregon Green 488 goat anti-mouse secondary antibody (Invitrogen) to label dopaminergic neurons, and counterstained with DAPI to identify cortical layers. For each animal, 7–10 images at the level of the SN and of the PFC (layer V-VI) were acquired for the DAPI, red, and green channels at 60× magnification with a Nikon A1 confocal microscope. Each image was a projection of a *Z*-stack with 20 *Z*-steps at 0.5 μm intervals. Lipofuscin inclusion bodies were visualized as red autofluorescent granules with the 561 nm laser excitation and analysis of their volume was performed using Imaris 7.2.3 software (Bitplane, Scientific Software).

Results

Age-related decrease in D-aspartate levels mirrors progressive increased expression in *Ddo* mRNA in the mouse brain

It has been reported that in the human and rat brain free D-Asp concentration decreases after birth and remains at low levels throughout postnatal life (Hashimoto et al., 1993; Schell et al., 1997; Sakai et al., 1998; Wolosker et al., 2000). Here we sought to investigate whether such ontogenetic variations occur also in the mouse brain. In this regard, we quantified the content of both free D-Asp and L-Asp in brain homogenates at different time points, between embryonic day 15 (E15) and adult postnatal day 60 (P60) by HPLC. At E15, the concentration of D-Asp and L-Asp detected in whole-brain homogenates were 5.10 ± 0.63 and 25.33 ± 4.13 nmol/mg protein, respectively. Consistently to humans and rats (Dunlop et al., 1986; Neidle and Dunlop, 1990; Hashimoto et al., 1993, 1995; Sakai et al., 1998; Wolosker et al., 2000), free D-Asp content in the mouse brain decreased significantly after birth (one-way ANOVA, $F_{(6,18)} = 9.394$; $p < 0.0001$; Fig. 1*c*). *Post hoc* comparison revealed a significant drop in free D-Asp concentration at P7 (3.45 ± 0.20 nmol/mg protein; $p = 0.0192$, compared with E15), followed by a progressive decrease at subsequent developmental stages until P60 (1.81 ± 0.28 nmol/mg protein; $p = 0.0343$, compared with P7; $p < 0.0001$, compared with E15; Fig. 1*c*). On the other hand, no changes were detected in free L-Asp levels at the analyzed ages ($F_{(6,18)} = 0.586$; $p = 0.7374$; Fig. 1*d*). Accordingly, the calculated D-Asp/total Asp ratio showed the same reduction profile observed for D-Asp during postnatal development ($F_{(6,18)} = 4.215$; $p = 0.0080$; Fig. 1*e*).

At the same prenatal and postnatal time points, we also investigated *Ddo* gene expression by qRT-PCR (Fig. 1*f*). Notably, the *Ddo* mRNA in the whole brain strongly increased during postnatal development (one-way ANOVA, $F_{(6,14)} = 14.751$; $p < 0.0001$). In particular, the relative expression of *Ddo* transcript was very low at E15 and P0 (0.03 ± 0.01 and 0.07 ± 0.02, respectively), and progressively raised during postnatal stages, reaching a ~25-fold increase at P60, compared with E15 (0.85 ± 0.10; $p < 0.0001$, Fisher's *post hoc*) (Fig. 1*f*). Finally, we evaluated the spatial pattern of *Ddo* mRNA transcriptional activation in the mouse brain during ontogenesis by ^{35}S radioactive ISH (Fig. 1*g*). At E15 and P0, *Ddo* mRNA expression was detected within the ependymal cell layer of the telencephalic ventricles. At P14, several brain regions, such as the hippocampus, thalamus, and cerebellum, displayed intense *Ddo* mRNA expression in addition to the ependymal cell layer. At P30 and, more robustly at P60, *Ddo* transcript levels strongly increased in these areas and appeared pronounced also in the midbrain region, pons, olfactory bulbs, and cortex. In addition to high-intensity signal in specific regional districts, we observed in adults a widespread expression of *Ddo* mRNA throughout the brain.

The state of methylation of the *Ddo* promoter controls *Ddo* mRNA expression in the mouse brain

The temporal increase of *Ddo* transcript levels observed by qRT-PCR and ISH (Fig. 1*f*,*g*) is coherent with the progressive global decrease of free D-Asp found in the brain during the postnatal life (Fig. 1*c*). This evidence prompted us to investigate the regulatory mechanism of *Ddo* expression in the mouse brain. In particular, we evaluated whether the age-related increase in cerebral *Ddo* mRNA could be explained by epigenetic modifications occurring during the late phases of embryogenesis and/or the early postna-

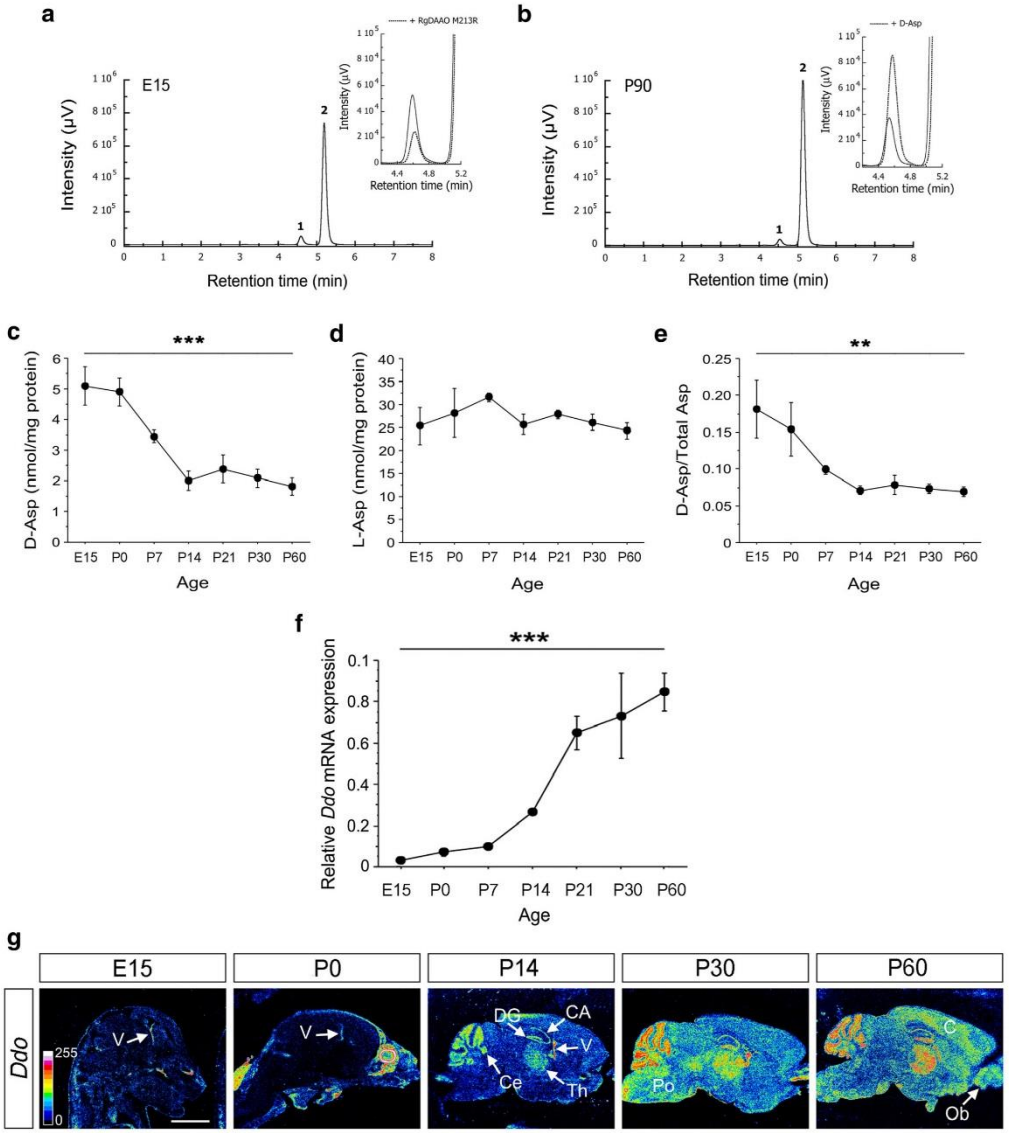

Figure 1. Variation in D-aspartate levels and *Ddo* mRNA expression in the mouse brain during ontogenesis. ***a***, ***b***, Examples of HPLC chromatograms illustrating the detection of (1) D-aspartate (D-Asp) and (2) L-aspartate (L-Asp) obtained from (***a***) E15 and (***b***) P90 brain tissue samples. The identity of the peak corresponding to D-aspartate (4.66 ± 0.09 min) was verified by treating E15 samples with 10 μg *RgDAAO* M213R (***a***, inset, dotted line), and by adding the external standard to P90 samples (***b***, inset, dotted line). D-Aspartate retention time is reported as the mean ± SD; $n = 34$. ***c–e***, Average content of D-aspartate, L-aspartate, and D-aspartate/total aspartate ratio in total brain of C57BL/6J mice at different ages (E15, $n = 5$; P0, $n = 2$; P7, $n = 3$; P14, $n = 6$; P21, P30, and P60, $n = 3$). The amount of (***c***) D-aspartate and (***d***) L-aspartate in the brain homogenates, detected by HPLC, was normalized by the total protein content of each sample. ***f***, Analysis of *Ddo* mRNA expression performed by qRT-PCR on a different set of whole brains from C57BL/6J mice at different ages ($n = 3$ per age). Quantity means of transcript were normalized to β-actin housekeeping gene. $^{**}p < 0.01$ (one-way repeated-measures ANOVA). $^{***}p < 0.0001$ (one-way repeated-measures ANOVA). Data are mean ± SEM. ***g***, Representative pseudocolor autoradiographs from sagittal sections throughout the mouse brain at E15, P0, P14, P30, and P60 showing *Ddo* mRNA expression pattern. The relationship between autoradiographic signal intensity (from 0 to 255) and the pseudocolor images is scaled by pseudocolor bars (from blue to white). Scale bar, 750 μm. V, Ependymal cell layer of the ventricle; CA, cornu ammonis area; Ce, cerebellum; DG, dentate gyrus; Th, thalamus; Po, pons; C, cortex; Ob, olfactory bulb.

tal stages of development. In this regard, we investigated the methylation state of the putative promoter region of the *Ddo* gene at different prenatal and postnatal developmental stages, from E15 to P60, using the same whole brain samples tested for *Ddo* mRNA quantification (Fig. 1*f*). DNA methylation analysis was assessed through a strategy based on the locus-specific amplification of bisulfite-treated genomic DNA. We covered two overlapping genomic regions surrounding the transcription start site (TSS): *Ddo* regulatory region 1 (RR1), spanning nucleotides −443 to 88 and including 6 CpG sites (positions −363, −330, −318, −242, −175, −125), and *Ddo* regulatory region 2 (RR2) spanning nucleotides −185 to 150 and including 4 CpG sites (positions −175, −125, 50, 113), the first two of which coincided with the last two located most 3′ in RR1 (Fig. 2*a*). At each CpG site, we observed that the methylation degree progressively decreased from E15 to adult stages (one-way ANOVA, $p = 0.0003$ for CpG 113, $p < 0.0001$ for all other CpG sites) (Fig. 2*b*). On average, the methylation state of the 8 CpG sites lying in the *Ddo* gene region from nucleotides −363 to 113 gradually decreased from ~60% in E15 brains to ~30% at P21-P60 stages ($F_{(6,14)} = 39.887$; $p < 0.0001$; Fig. 2*c*). Overall, these results for the first time highlight the occurrence of a developmentally regulated DNA demethylation process at the putative *Ddo* gene promoter.

To assess whether the progressive demethylation of the *Ddo* regulatory region could influence the gradual postnatal increase in *Ddo* mRNA levels, we then investigated whether "forced" alteration in DNA methylation state was linked to variations in cerebral *Ddo* expression. To this aim, we treated E17 cortical neurons (in which *Ddo* transcript is at the lowest expression level) either with vehicle or 5 μM 5-aza-2-deoxycytidine (azacitidine), a drug known to promote DNA demethylation both in cycling and in postmitotic cells (Marutha Ravindran and Ticku, 2005; Nelson et al., 2008; Gavin et al., 2013). Consistent with an epigenetic control of DNA methylation on *Ddo* mRNA transcription, qRT-PCR analysis showed that treatment with azacitidine caused an ~4-fold increase in transcriptional levels of *Ddo* (relative expression: 3.97 ± 0.93), compared with vehicle-treated neurons (Fig. 2*d*).

Absence of DDO is associated with higher extracellular concentration of free D-aspartate in the brain of *Ddo*$^{-/-}$ mice

In the attempt to decipher the physiological relevance of the postnatal *Ddo* promoter demethylation and, in turn, the influence of the concomitant *Ddo* mRNA upregulation on free D-Asp occurrence, we analyzed the neurochemical features of *Ddo*$^{-/-}$ adult brains. We used this animal model because it maintains, along the entire postnatal life, the physiological condition occurring during embryonic stages, when cerebral *Ddo* expression is suppressed and free D-Asp is abundant. Consistently, our ^{35}S-radioactive ISH revealed that E15 *Ddo*$^{+/+}$ and *Ddo*$^{-/-}$ brains were almost indistinguishable, as *Ddo* mRNA appeared barely detectable in both genotypes; in contrast, at P60, *Ddo*$^{-/-}$ brains maintained an "embryo-like" inconsistent *Ddo* expression, whereas *Ddo*$^{+/+}$ brains displayed robust and widespread *Ddo* mRNA detection (Fig. 3*a*).

Based on the lack of *Ddo* expression in knock-out brains, we measured the total amount of free D-Asp and L-Asp in the PFC of *Ddo*$^{-/-}$ mice. As previously reported in other brain regions (Errico et al., 2006; Huang et al., 2006; Han et al., 2015), HPLC analysis indicated that also in the PFC the deletion of the *Ddo* gene yielded a strong increase in total D-Asp levels, compared with controls (~30-fold) (*Ddo*$^{+/+}$: 0.49 ± 0.04 nmol/mg protein, *Ddo*$^{-/-}$: 15.91 ± 1.46 nmol/mg protein; $p < 0.0001$, Student's *t* test; Fig. 3*b*), whereas L-Asp content remained unchanged between genotypes (*Ddo*$^{+/+}$: 25.88 ± 2.10 nmol/mg protein, *Ddo*$^{-/-}$: 25.37 ± 1.21 nmol/mg protein; $p = 0.8397$; Fig. 3*c*). In agreement with these detections, an increase of the same magnitude as for D-Asp was also found for the D-Asp/total Asp ratio in *Ddo*$^{-/-}$ mice, compared with *Ddo*$^{+/+}$ littermates (*Ddo*$^{+/+}$: 0.019 ± 0.001, *Ddo*$^{-/-}$: 0.38 ± 0.02; $p < 0.0001$; Fig. 3*d*).

Then, we measured free D-Asp extracellular levels in the PFC of freely moving *Ddo*$^{+/+}$ and *Ddo*$^{-/-}$ mice by *in vivo* microdialysis, followed by HPLC analysis of the collected perfusates, as reported by Guida et al. (2015). Remarkably, we found that lack of *Ddo* resulted in significantly ~5-fold higher free D-Asp extracellular levels in the cortical perfusates of *Ddo*$^{-/-}$ mice, compared with *Ddo*$^{+/+}$ animals (mean values: *Ddo*$^{+/+}$, 18.26 ± 4.40 nM; *Ddo*$^{-/-}$, 101.50 ± 8.41 nM; two-way ANOVA with repeated measures, genotype effect: $F_{(1,56)} = 20.034$, $p = 0.0005$; Fig. 3*e*). We finally collected the last dialysate fraction (150–180 min) in Ca^{2+}-free ACSF. Interestingly, under this condition, extracellular concentration of D-Asp was below the detection limit in both *Ddo*$^{+/+}$ and *Ddo*$^{-/-}$ mice, suggesting that the removal of Ca^{2+} from the ACSF is able to prevent the cortical efflux of free D-Asp (Fig. 3*e*). In addition to D-Asp, we also detected the extracellular cortical concentration of free L-Asp and L-Glu. Surprisingly, despite that total L-Asp content was comparable between genotypes (Fig. 3*c*), a significant ~2-fold increase of extracellular L-Asp levels was apparent in the PFC of *Ddo*$^{-/-}$ mice, compared with wild-type ones (mean values: *Ddo*$^{+/+}$, 84.00 ± 2.44 nM; *Ddo*$^{-/-}$, 177.16 ± 8.74 nM; $F_{(1,56)} = 14.954$, $p = 0.0017$; Fig. 3*f*). On the other hand, extracellular L-Glu concentrations detected in cortical perfusates were comparable between genotypes (mean values: *Ddo*$^{+/+}$, 1.02 ± 0.03 μM, *Ddo*$^{-/-}$, 0.86 ± 0.03 μM; $F_{(1,32)} = 0.399$, $p = 0.5451$; Fig. 3*g*). As observed for D-Asp, extracellular levels of both L-Asp and L-Glu were undetectable when microdialysis was performed in a Ca^{2+}-free ACSF (Fig. 3*f*,*g*).

Nonphysiological increase of D-aspartate in *Ddo*$^{-/-}$ brains is associated with age-related caspase-3 activation and cell death in the prefrontal cortex

Several works have indicated that free D-Asp activates NMDAR-dependent signaling and currents (Errico et al., 2015b). On the other hand, it is known that persistent stimulation of NMDARs at extrasynaptic site triggers oxidative stress and the activation of apoptotic/necrotic pathways (Lipton, 2008; Hardingham and Bading, 2010; Parsons and Raymond, 2014). Here, we examined whether constitutive exposure of cortical neurons to nonphysiological, higher extracellular D-Asp levels produces neurotoxic effects in the brain of *Ddo*$^{-/-}$ mice during aging. Considering that caspase activation plays a pivotal role in neuronal apoptosis and represents the terminal event preceding cell death (Shalini et al., 2015), we measured the expression of active caspase-3 and DNA fragmentation by TUNEL staining in the infralimbic/prelimbic area of the PFC in *Ddo*$^{-/-}$ mice at 3, 6, and 13 months of age (Fig. 4). Two-way ANOVA revealed a significant age-dependent increase of caspase-3 activation in *Ddo*$^{-/-}$ mice (genotype, $F_{(1,12)} = 1236.720$, $p < 0.0001$; genotype × age, $F_{(2,12)} = 336.130$, $p < 0.0001$). More in detail, in line with detrimental effects of nonphysiological NMDAR stimulation produced by higher extracellular free D-Asp levels, we found a significantly increased percentage of activated caspase-3-positive cells in 6- and 13-month-old *Ddo*$^{-/-}$ mice, compared with age-matched controls (6-month-old: *Ddo*$^{+/+}$, 27.98 ± 0.59, *Ddo*$^{-/-}$, 62.87 ± 1.27; $p < 0.0001$; 13-month-old: *Ddo*$^{+/+}$, 26.29 ± 0.55, *Ddo*$^{-/-}$, 71.51 ± 0.55; $p < 0.0001$; Fisher's *post hoc*; Fig. 4*a*,*b*). The in-

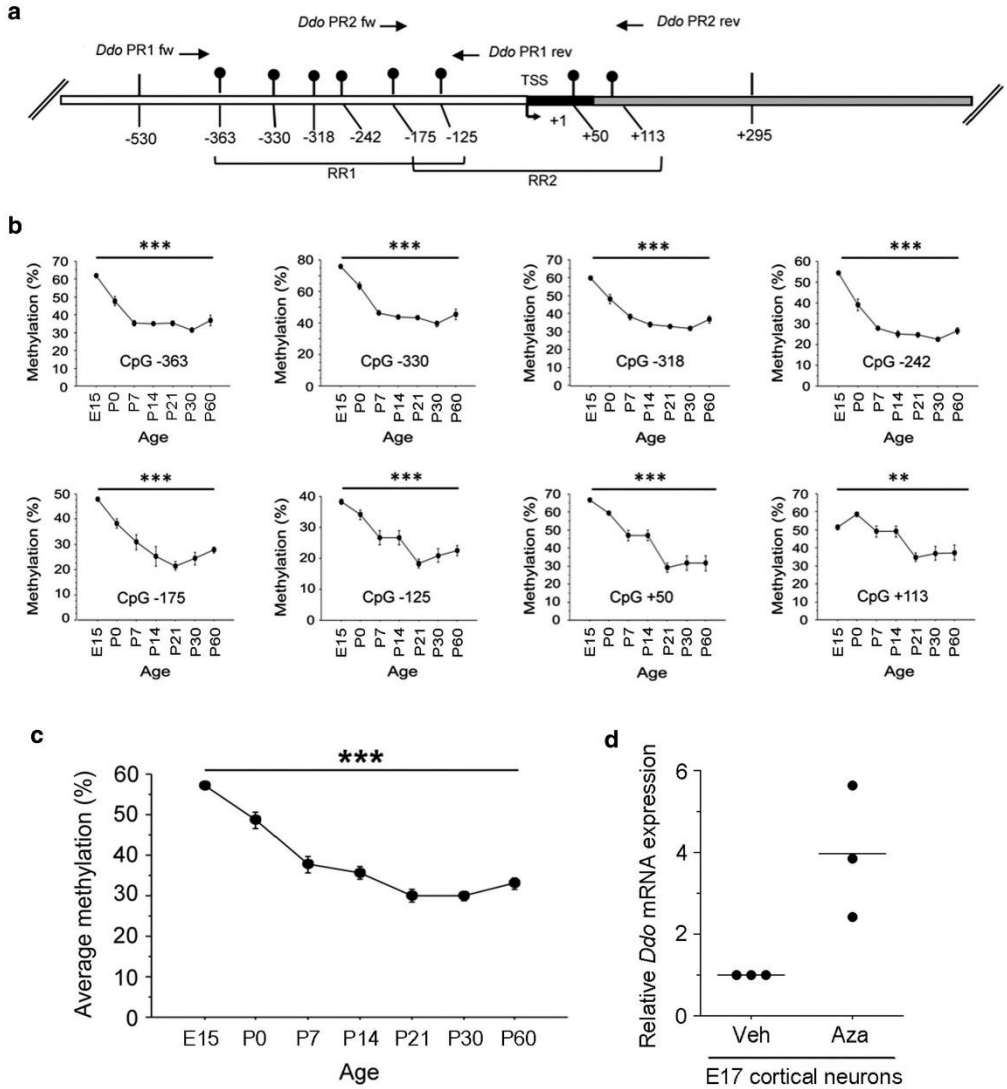

Figure 2. DNA methylation degree of the *Ddo* gene during mouse brain ontogenesis. ***a***, Structure of the putative mouse *Ddo* gene promoter. Arrow indicates the transcription start site (TSS, +1). White box represents the putative regulatory upstream region. Black box represents exon 1. Gray box represents first intron. Position of CpG sites is indicated as relative to TSS. Position of the primers used for bisulfite analysis is indicated by arrows at the top of the map (*Ddo* PR1 fw, *Ddo* PR1 rev, and *Ddo* PR2 fw, *Ddo* PR2 rev). RR1 and RR2 indicate the amplicons used to analyze the regulatory region 1 and 2, respectively. ***b***, ***c***, Graphs represent the percentage of methylation in (***b***) the single CpG sites and (***c***) the average methylation degree of the eight CpG sites included in the RR1 and RR2 regions, at the indicated developmental stages. Whole-brain samples used for the methylation analysis are the same as that used to measure *Ddo* mRNA relative expression (Fig. 1*f*). ***d***, Relative *Ddo* mRNA expression in primary cortical neurons obtained from E17 brains of C57BL/6J mice, treated with vehicle (Veh) or 5 μM 5-aza-2′-deoxycytidine (azacitidine, Aza) for 48 h. $^{**}p < 0.01$ (one-way repeated-measures ANOVA). $^{***}p < 0.0001$ (one-way repeated-measures ANOVA). Data are mean ± SEM.

crease of percentage of activated caspase-3-positive cells was mainly attributed to the pyramidal neurons of the PFC as observed by a reduction of the number of NeuN-immunoreactive profile and by increased percentage of activated caspase-3/NeuN immunocoexpression within the NeuN-positive neurons of 13-month-old $Ddo^{-/-}$ mice ($Ddo^{+/+}$, 20.56 ± 2.04%, $Ddo^{-/-}$, 67.45 ± 2.30%; $p < 0.0001$; Student's *t* test; Fig. 4*a*, bottom panels).

In agreement with the substantial increase of active caspase-3 found in $Ddo^{-/-}$ mice, we also detected a robust age-dependent

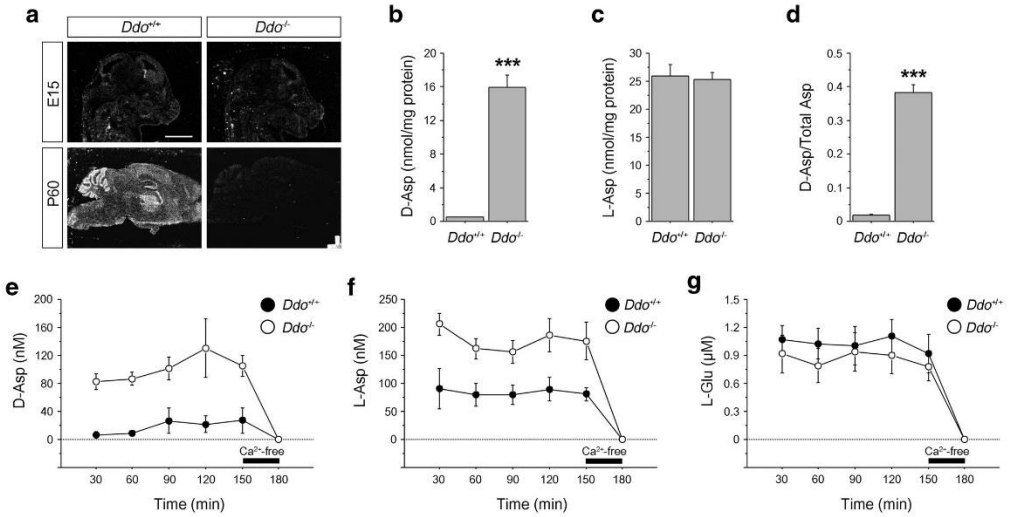

Figure 3. Increased extracellular levels of D-aspartate in the prefrontal cortex of *Ddo* $^{-/-}$ mice. ***a***, Representative darkfield autoradiograms of sagittal sections showing *Ddo* mRNA expression in the brain of *Ddo* $^{+/+}$ and *Ddo* $^{-/-}$ mice at E15 and P60. Scale bar, 750 μm. ***b–d***, D-aspartate (D-Asp) and L-aspartate (L-Asp) content in prefrontal cortex homogenates of *Ddo* $^{+/+}$ and *Ddo* $^{-/-}$ mice ($n = 5$ per genotype), measured by HPLC. The average amounts of (***b***) D-aspartate and (***c***) L-aspartate detected during the analyses were normalized by the total protein content in the tissue samples or (***d***) reported as D-aspartate/total aspartate ratio. ***$p < 0.0001$, compared with *Ddo* $^{+/+}$ mice (Student's *t* test). ***e–g***, Average extracellular concentration of (***e***) D-aspartate, (***f***) L-aspartate, and (***g***) L-glutamate (L-Glu) measured by HPLC in dialysates collected from the prefrontal cortex of freely moving *Ddo* $^{+/+}$ and *Ddo* $^{-/-}$ mice ($n = 8$ for D-aspartate and L-aspartate detection, $n = 5$ for L-glutamate detection) at different time-points (30–180 min). Last fraction of dialysates (150–180 min) was collected in a Ca^{2+}-free ACSF. Amino acid extracellular levels are expressed as nM (D-aspartate and L-aspartate) or μM (L-glutamate) concentration. Data are mean ± SEM.

activation of apoptotic events in the infralimbic/prelimbic area of these animals (genotype, $F_{(1,12)} = 1157.068$, $p < 0.0001$; genotype × age, $F_{(2,12)} = 286.507$, $p < 0.0001$). Indeed, subsequent *post hoc* analysis revealed a significantly higher percentage of TUNEL-positive cells in 6- and 13-month-old *Ddo* $^{-/-}$ mice, compared with age-matched *Ddo* $^{+/+}$ animals (6-month-old: *Ddo* $^{+/+}$, 27.03 ± 1.76, *Ddo* $^{-/-}$, 78.66 ± 1.35; $p < 0.0001$; 13-month-old: *Ddo* $^{+/+}$, 25.88 ± 1.22, *Ddo* $^{-/-}$, 79.29 ± 1.01; $p < 0.0001$; Fig. 4*c*,*d*).

Increased levels of D-aspartate in *Ddo* $^{-/-}$ brains are associated with age-related appearance of dystrophic microglia in the substantia nigra

We recently found that exogenous application of free D-Asp mainly triggers NMDAR-dependent currents in dopaminergic neurons of the substantia nigra pars compacta (Krashia et al., 2015). Based on this observation, we used *Ddo* $^{-/-}$ mice to explore whether also in the SN the physiological activity of DDO is able to prevent neurotoxic insults produced by persistently elevated free D-Asp during aging.

Before starting such characterization, we first measured free D-Asp levels in the ventral midbrain of adult *Ddo* $^{+/+}$ and *Ddo* $^{-/-}$ mice by HPLC. In line with the expression of *Ddo* in this cerebral area (Fig. 1*g*), we found a significant ~5-fold increase in free D-Asp content in *Ddo* $^{-/-}$ brains, compared with controls (*Ddo* $^{+/+}$: 1.30 ± 0.10 nmol/mg protein, *Ddo* $^{-/-}$: 5.82 ± 0.24 nmol/mg protein; $p < 0.0001$, Student's *t* test; Fig. 5*a*). Conversely, no significant change between genotypes was detected in free L-Asp levels (*Ddo* $^{+/+}$: 30.19 ± 1.51 nmol/mg protein; *Ddo* $^{-/-}$: 34.57 ± 1.95 nmol/mg protein; $p = 0.1261$; Fig. 5*b*). Accordingly, the D-Asp/total Asp ratio significantly increased in the midbrain of *Ddo* $^{-/-}$ animals, compared with *Ddo* $^{+/+}$ littermates (*Ddo* $^{+/+}$: 0.041 ± 0.001; *Ddo* $^{-/-}$: 0.145 ± 0.008; $p < 0.0001$; Fig. 5*c*).

Then, to assess the involvement of DDO in the physiological aging process of midbrain dopaminergic neurons, we analyzed in the SN of *Ddo* $^{-/-}$ mice the number and morphology of microglial cells (Fig. 5*d–g*), whose activation is considered as a reliable marker of neuronal inflammatory/neurotoxic conditions (Streit et al., 2009). To this aim, we used mice at different ages, ranging from 0.5 to 13 months. Statistical analysis revealed a significant effect of genotype on the total number of microglial cells (two-way ANOVA, $F_{(1,20)} = 7.803$, $p = 0.0002$; Fig. 5*d*). Subsequent *post hoc* analysis showed a significantly higher number of total microglia (mostly resting phenotype) in 0.5-, 3-, 10-, and 13-month-old *Ddo* $^{-/-}$ mice, compared with their respective age-matched controls (0.5-month-old: *Ddo* $^{+/+}$, 1.38 ± 0.15 cells/20,000 μm^2; *Ddo* $^{-/-}$, 2.76 ± 0.30 cells/20,000 μm^2, $p = 0.0147$; 3-month-old: *Ddo* $^{+/+}$, 1.66 ± 0.19 cells/20,000 μm^2; *Ddo* $^{-/-}$, 3.00 ± 0.38 cells/20,000 μm^2, $p = 0.0366$; 10-month-old: *Ddo* $^{+/+}$, 2.28 ± 0.15 cells/20,000 μm^2; *Ddo* $^{-/-}$, 3.66 ± 0.10 cells/20,000 μm^2, $p = 0.0014$; 13-month-old: *Ddo* $^{+/+}$, 2.33 ± 0.10 cells/20,000 μm^2; *Ddo* $^{-/-}$, 2.83 ± 0.10 cells/20,000 μm^2, $p = 0.0212$; Fig. 4*d*).

Further, we assessed the number of reactive microglia, that resulted to be differentially activated in *Ddo* $^{+/+}$ and *Ddo* $^{-/-}$ mice during aging (two-way ANOVA: genotype, $F_{(1,20)} = 7.816$, $p = 0.0112$; genotype × age, $F_{(4,20)} = 3.552$, $p = 0.0241$; Figure 5*e*). Indeed, we found an increasing trend in the number of reactive microglia in *Ddo* $^{-/-}$ mice at 3, 6, and 10 months of age (3-month-old: *Ddo* $^{+/+}$, 0.11 ± 0.11 cells/20,000 μm^2; *Ddo* $^{-/-}$, 0.78 ± 0.22 cells/20,000 μm^2, $p = 0.055$; 6-month-old: *Ddo* $^{+/+}$,

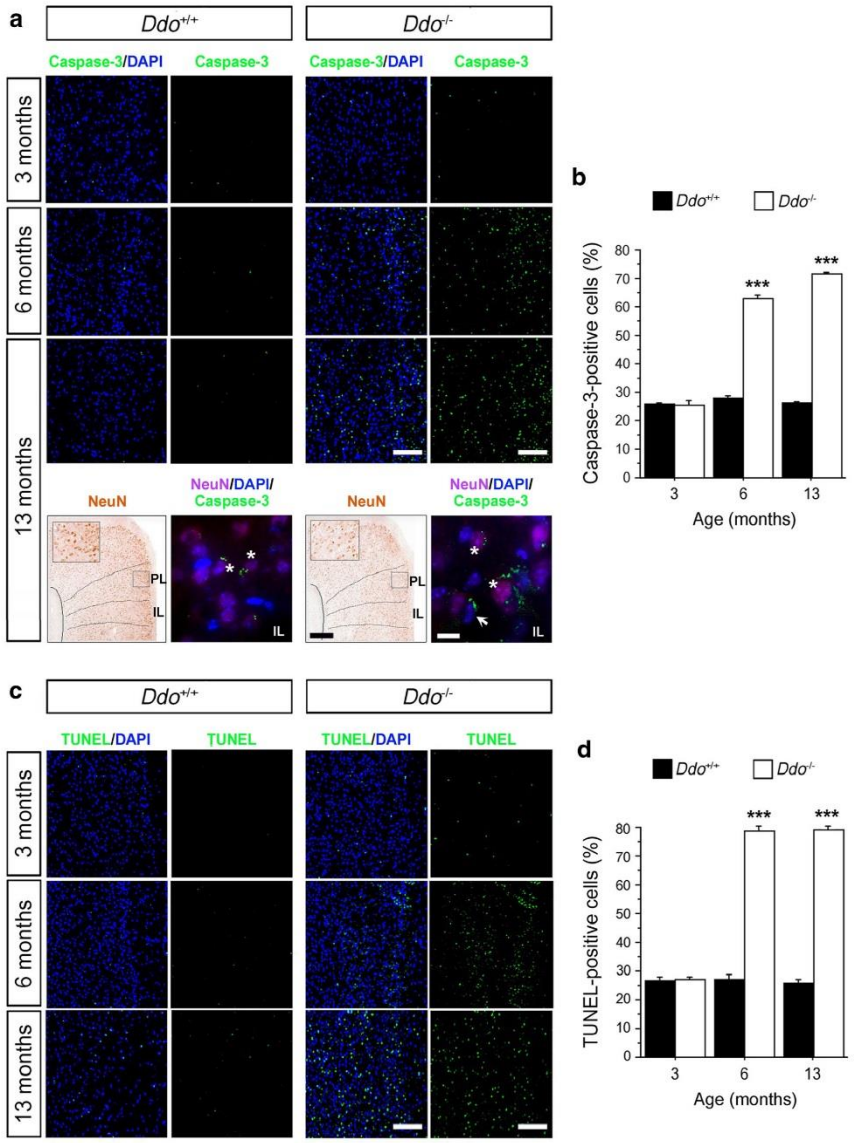

Figure 4. Precocious activation of caspase-3 and cell death in the prefrontal cortex of *Ddo* $^{-/-}$ mice. ***a–d***, Analysis of apoptotic markers in pyramidal neurons of the prefrontal cortex of 3-, 6-, and 13-month-old *Ddo* $^{+/+}$ and *Ddo* $^{-/-}$ mice ($n = 3$ per genotype and age). ***a***, Representative images showing activated caspase-3 (green) immunoreactivity in laminae II/III of the infralimbic cortex of *Ddo* $^{+/+}$ and *Ddo* $^{-/-}$ mice. Nuclei are counterstained with DAPI (blue). Bottom panels, Representative NeuN immunoperoxidase in 13-month-old mice. Inset, High magnification of the boxed area in the prelimbic (PL) region showing the reduction of number of NeuN-immunoreactive profiles in *Ddo* $^{-/-}$ mice, compared with *Ddo* $^{+/+}$ littermates. High magnification of NeuN/DAPI/caspase-3 immunofluorescence in laminae II/III of the infralimbic (IL) cortex of 13-month-old mice. Asterisks and arrow indicate caspase-3 immunoreactivity in neurons and in some non-neuronal cells, respectively. ***c***, TUNEL staining (green) immunoreactivity in laminae II/III of the infralimbic cortex of *Ddo* $^{+/+}$ and *Ddo* $^{-/-}$ mice. Nuclei are counterstained with DAPI (blue). Scale bars: NeuN, 500 μm; caspase-3, caspase3/DAPI, TUNEL, TUNEL/DAPI, 100 μm; NeuN/DAPI/caspase-3, 8 μm. ***b***, ***d***, Bar graphs showing the percentage of (***b***) caspase-3- and (***d***) TUNEL-positive cells. ***$p < 0.0001$, compared with *Ddo* $^{+/+}$ mice (Fisher's *post hoc*). Data are mean ± SEM.

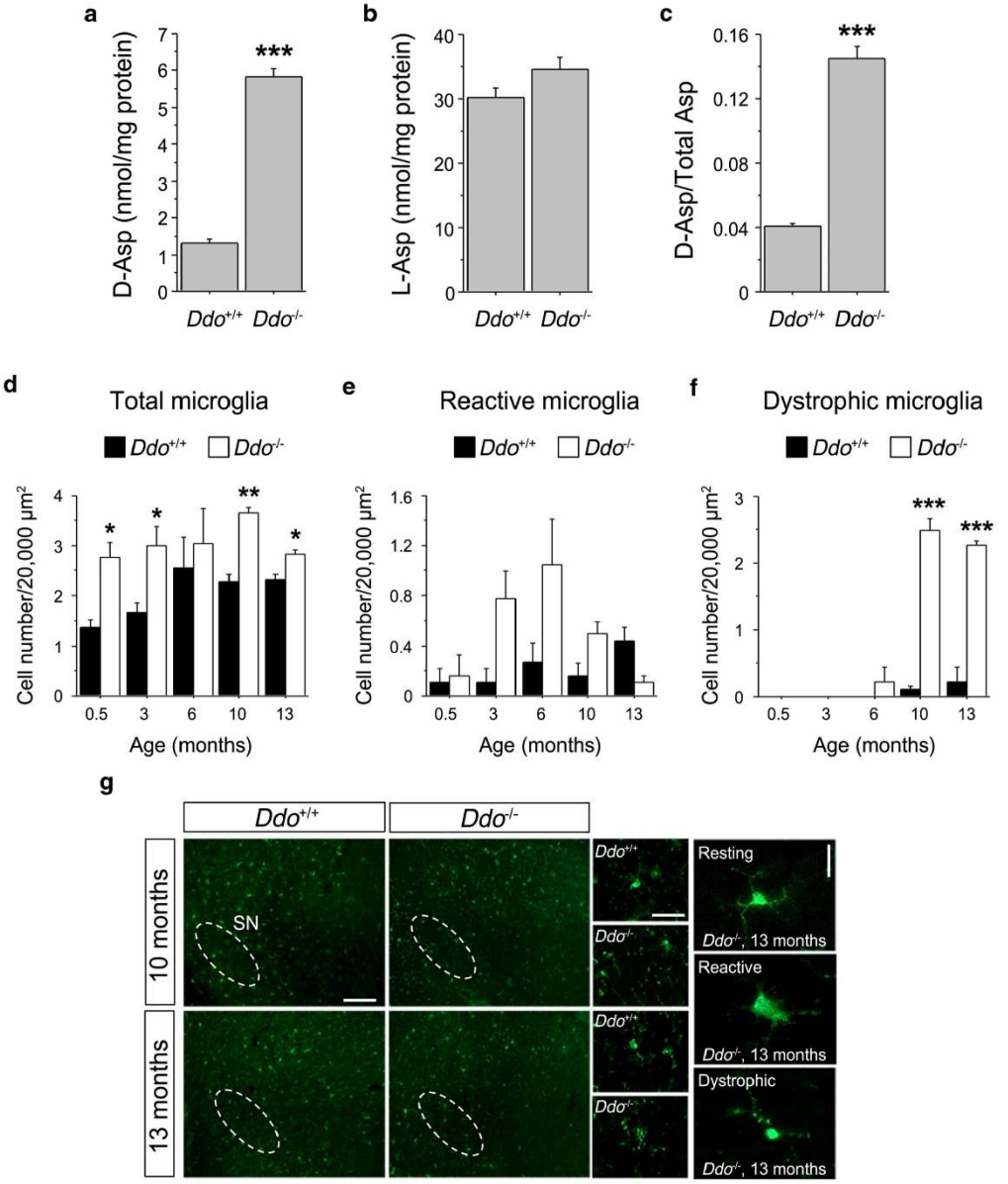

Figure 5. D-Aspartate detection in total homogenates and precocious appearance of dystrophic microglia in the midbrain of *Ddo* $^{-/-}$ mice. ***a–c***, D-Aspartate (D-Asp) and L-aspartate (L-Asp) content in midbrain homogenates from *Ddo* $^{+/+}$ and *Ddo* $^{-/-}$ mice ($n = 4$ per genotype), measured by HPLC analysis. The average amounts of (***a***) D-aspartate and (***b***) L-aspartate detected during the analyses were normalized by the total protein content in the tissue samples or (***c***) reported as the D-aspartate/total aspartate ratio. ***$p < 0.0001$, compared with *Ddo* $^{+/+}$ mice (Student's *t* test). ***d–g***, Morphological analysis of microglia in the substantia nigra of *Ddo* $^{+/+}$ and *Ddo* $^{-/-}$ mice during ontogenesis ($n = 3$ per genotype and age), evaluated by Iba-1 immunofluorescence. Quantitative analysis of the (***d***) total, (***e***) hypertrophic, and (***f***) dystrophic-like microglia at 0.5, 3, 6, 10, and 13 months of age. ***g***, Immunofluorescence of Iba-1-positive microglial cells in the substantia nigra of 10- and 13-month-old *Ddo* $^{+/+}$ and *Ddo* $^{-/-}$. At the lowest magnification, the region of the substantia nigra is delimited by a dotted oval. At the highest magnification, examples are shown of resting, reactive, and dystrophic-like microglia identified in the substantia nigra of 13-month-old *Ddo* $^{-/-}$ mice. Scale bars: 200, 50, 25 μm. *$p < 0.05$, compared with *Ddo* $^{+/+}$ mice (Fisher's *post hoc*). **$p < 0.01$, compared with *Ddo* $^{+/+}$ mice (Fisher's *post hoc*). ***$p < 0.0001$, compared with *Ddo* $^{+/+}$ mice (Fisher's *post hoc*). Data are mean ± SEM.

0.27 ± 0.15 cells/20,000 μm^2; $Ddo^{-/-}$, 1.05 ± 0.36 cells/20,000 μm^2, $p = 0.1186$; 10-month-old: $Ddo^{+/+}$, 0.16 ± 0.09 cells/20,000 μm^2; $Ddo^{-/-}$, 0.50 ± 0.10 cells/20,000 μm^2, $p = 0.0700$; Fig. 5*e*) and, conversely, a trend decline in 13-month-old knockouts, compared with wild-type littermates ($Ddo^{+/+}$, 0.44 ± 0.11 cells/20,000 μm^2; $Ddo^{-/-}$, 0.11 ± 0.06 cells/20,000 μm^2, $p = 0.0550$; Fig. 5*e*).

Finally, we counted the number of dystrophic microglia, characterized by fragmented cell body and processes, which is thought to be predictive of neuronal damage, as reported also in Alzheimer's disease human brain (Streit et al., 2009). Consistent with the neurotoxic effect of deregulated D-Asp levels, we found an age-related appearance of dystrophic microglia in the SN of $Ddo^{-/-}$ mice, which was not detected in $Ddo^{+/+}$ controls (two-way ANOVA: age, $F_{(4,20)} = 70.502$, $p < 0.0001$; genotype, $F_{(1,20)} = 165.302$, $p < 0.0001$; age × genotype, $F_{(4,20)} = 53.456$, $p < 0.0001$; Figure 5*f*). In particular, we evidenced a significant occurrence of dystrophic microglia specifically in 10- and 13-month-old $Ddo^{-/-}$ mice, compared with their respective age-matched controls (10-month-old: $Ddo^{+/+}$, 0.11 ± 0.05 cells/20,000 μm^2; $Ddo^{-/-}$, 2.50 ± 0.17 cells/20,000 μm^2, $p = 0.0002$; 13-month-old: $Ddo^{+/+}$, 0.22 ± 0.22 cells/20,000 μm^2 $Ddo^{-/-}$, 2.27 ± 0.06 cells/20,000 μm^2, $p = 0.0009$; Fig. 5*f*,*g*).

Increased levels of free D-aspartate trigger age-related caspase-3 activation and cell death in dopaminergic neurons of the substantia nigra

Based on the abnormal appearance of dystrophic microglia, we explored whether the constitutive upregulation of free D-Asp levels in $Ddo^{-/-}$ brains also triggered the activation of apoptotic pathway and cell death in TH-positive neurons of the SN. To this aim, we evaluated the expression levels of active caspase-3 in 0.5-, 3-, 6-, 10-, and 13-month-old $Ddo^{-/-}$ mice. Interestingly, we found a significant genotype-dependent variation in the percentage of active caspase-3-positive cells (two-way ANOVA: genotype, $F_{(1,20)} = 214.010$, $p < 0.0001$; age × genotype, $F_{(4,20)} = 22.902$, $p < 0.0001$). Accordingly, *post hoc* analysis revealed a higher expression of active caspase-3 already in 3-month-old and, more substantially, also in 6-, 10-, and 13-month-old knockout animals, compared with their respective age-matched controls (3-month-old: $Ddo^{+/+}$, 14.16 ± 1.12%, $Ddo^{-/-}$, 18.40 ± 0.81%, $p = 0.0375$; 6-month-old: $Ddo^{+/+}$, 18.57 ± 1.45%, $Ddo^{-/-}$, 36.66 ± 2.35%, $p = 0.0028$; 10-month-old: $Ddo^{+/+}$, 19.99 ± 2.05%, $Ddo^{-/-}$, 45.42 ± 0.50%, $p = 0.0003$; 13-month-old: $Ddo^{+/+}$, 19.34 ± 2.47%, $Ddo^{-/-}$, 49.52 ± 2.41%, $p = 0.0009$; Fig. 6*a*,*b*, arrows).

Finally, we detected TUNEL staining in the SN of 3-, 6-, and 13-month-old $Ddo^{-/-}$ mice. In agreement with previous results found in the PFC, we revealed that the number of TUNEL/TH-positive neurons in this brain region of $Ddo^{-/-}$ mice significantly increased with age (two-way ANOVA: genotype, $F_{(1,12)} = 214.764$, $p < 0.0001$; genotype × age, $F_{(2,12)} = 44.238$, $p < 0.0001$). The following *post hoc* analysis showed a higher percentage of positive cells in 6- and 13-month-old $Ddo^{-/-}$ mice, compared with age-matched controls (6-month-old: $Ddo^{+/+}$, 21.28 ± 1.06, $Ddo^{-/-}$, 41.65 ± 1.16, $p = 0.0002$; 13-month-old: $Ddo^{+/+}$, 21.83 ± 0.93, $Ddo^{-/-}$, 47.93 ± 1.75, $p = 0.0002$; Fig. 6*c*,*d*).

Overall, our data indicate that physiological enzymatic activity of DDO in the brain has a relevant neuroprotective effect able to prevent abnormal accumulation of extracellular free D-Asp that would otherwise trigger precocious degenerative events during aging.

Increased extracellular levels of free D-aspartate elicit precocious age-related accumulation of lipofuscin in $Ddo^{-/-}$ brains

To investigate the presence of oxidative stress as a consequence of persistent upregulation of free D-Asp levels, we assessed in $Ddo^{-/-}$ mice the levels of lipofuscin deposition, an autofluorescent pigment that accumulates over time and that positively correlates with the rate of aging (Brunk and Terman, 2002; Riga et al., 2006). Interestingly, lipofuscin accumulation was not yet detectable either in the SN (Fig. 7*a*) or in the PFC (data not shown) of both genotypes at preweaning stage (0.5 months). Conversely, in both the SN and in the layers V-VI of the PFC of adult $Ddo^{-/-}$ animals (3 months), we observed a significant increase of the total volume of lipofuscin inclusion bodies compared with $Ddo^{+/+}$ mice (Fig. 7*a*,*b*; $p < 0.05$, Student's *t* test). The precocious accumulation of lipofuscin in the $Ddo^{-/-}$ brain suggests that persistent elevation of D-Asp levels triggers greater oxidative stress and further supports the role of aberrant D-Asp metabolism on the early neurodegenerative events found in mutants.

Discussion

In the present work, we first demonstrated conserved age-related reduction of free D-Asp levels in the mouse brain, in line with previous observations in rats and humans (Hashimoto et al., 1993; Schell et al., 1997; Sakai et al., 1998; Wolosker et al., 2000). In addition, we showed a remarkable age-related increase in *Ddo* mRNA levels that is in line with the previously reported postnatal enhancement in DDO activity (Van Veldhoven et al., 1991) and the progressive decrease in free D-Asp levels. This evidence suggests that the ontogenetic changes in *Ddo* mRNA expression are most likely able to control, as net effect, the actual concentration of free D-Asp in the brain. Consistently, we have recently found that reduced levels of free D-Asp in the PFC of patients with schizophrenia (Errico et al., 2013) are associated with increased levels of *Ddo* mRNA, compared with healthy subjects (Errico et al., 2015b). Interestingly, we also found that the temporal increase in postnatal *Ddo* mRNA levels is mirrored by a concomitant and progressive demethylation of *Ddo* gene regulatory region surrounding the TSS. To unveil the causal relationship between demethylation of the putative *Ddo* promoter and increased *Ddo* transcription, we tested the effect of the DNA-demethylating agent azacitidine in primary neuronal culture from embryonic brain, when the physiological expression of this gene is nearly undetectable. Interestingly, the evidence that azacitidine induces an ~4-fold increase in *Ddo* mRNA levels, compared with vehicle-treated controls, indicates the existence of a finely tuned demethylation process at the basis of the observed postnatal increase in *Ddo* gene expression. In this view, we argue that the epigenetic changes within the *Ddo* regulatory region herein investigated are part of a developmental program to regulate the timed expression of the *Ddo* gene during prenatal and postnatal brain development. On the other hand, ISH clearly indicated that postnatal transcriptional activation of *Ddo* gene differs from one brain area to another, suggesting that *Ddo* promoter demethylation occurs with a peculiar spatiotemporal pattern to properly regulate the regional postnatal occurrence of DDO and, ultimately, free D-Asp concentrations.

Despite pharmacological, neurophysiological, and behavioral data indirectly asserting a role for free D-Asp in modulating glutamatergic system (Errico et al., 2012, 2015a), the basal cerebral content of this D-amino acid has long been considered too low to justify a neurobiological implication at adulthood. Herein, by

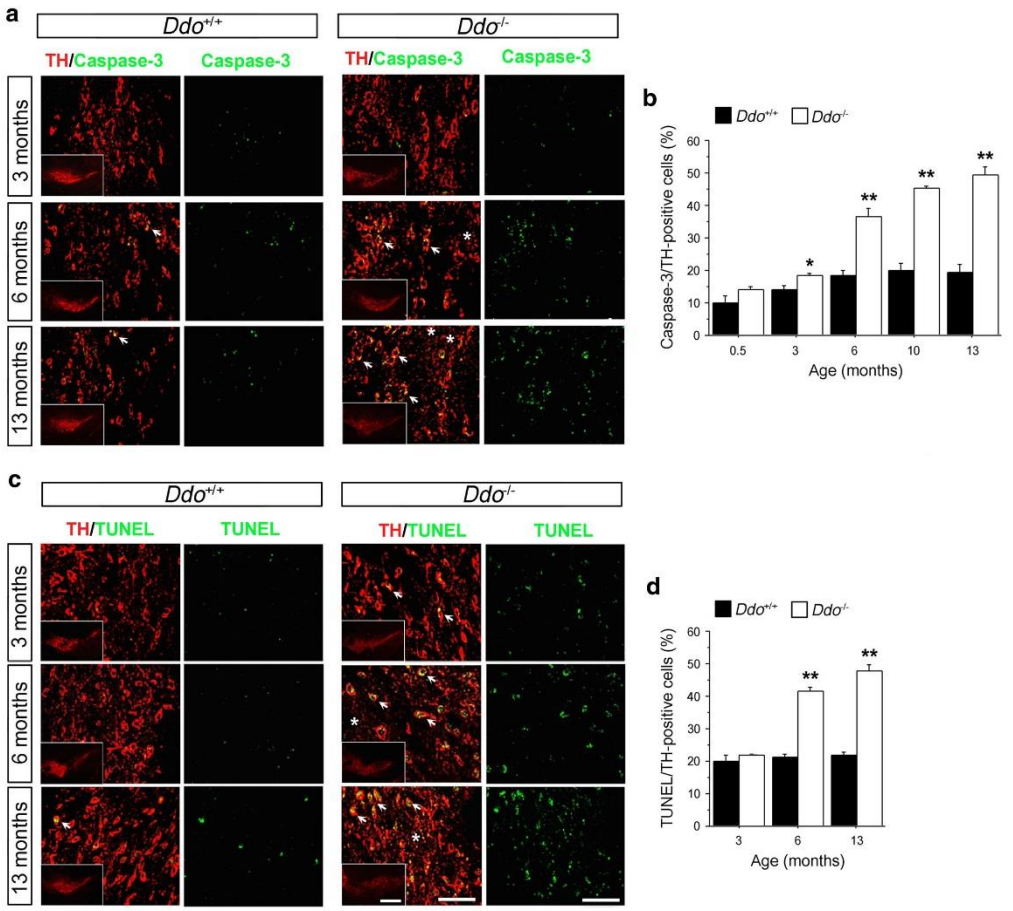

Figure 6. Precocious activation of caspase-3 and cell death in the substantia nigra of *Ddo* $^{-/-}$ mice. ***a–d***, Analysis of apoptotic markers in TH-positive neurons of the substantia nigra of *Ddo* $^{+/+}$ and *Ddo* $^{-/-}$ mice during ontogenesis ($n = 3$ per genotype and age). ***a***, ***c***, Representative images showing (***a***) activated caspase-3 immunoreactivity or (***c***) TUNEL staining immunoreactivity in TH-positive neurons from 3-, 6-, and 13-month-old *Ddo* $^{+/+}$ and *Ddo* $^{-/-}$ mice ($n = 3$ per genotype and age). Arrows indicate some of these neurons. Asterisks indicate representative areas, including TH-positive neuronal apoptotic debris. Insets, Low magnifications of the substantia nigra showing a significant reduction of TH immunodensity in *Ddo* $^{-/-}$, compared with *Ddo* $^{+/+}$ mice, more evident in aged *Ddo* $^{-/-}$ mice. Scale bars: insets, 200 μm; TH/caspase-3, caspase-3, TH/TUNEL, TUNEL, 50 μm. ***b***, ***d***, Bar graphs represent the percentage of (***b***) caspase-3/TH-positive cells (0.5-, 3-, 6-, 10-, and 13-month-old *Ddo* $^{+/+}$ and *Ddo* $^{-/-}$ mice) or (***d***) TUNEL/TH-positive cells (3-, 6-, and 13-month-old *Ddo* $^{+/+}$ and *Ddo* $^{-/-}$ mice). *$p < 0.05$, compared with *Ddo* $^{+/+}$ mice (Fisher's *post hoc*). **$p < 0.01$, compared with *Ddo* $^{+/+}$ mice (Fisher's *post hoc*). Data are mean ± SEM.

means of microdialysis studies performed in the PFC of freely moving animals, we demonstrated the occurrence of nanomolar concentrations of extracellular free D-Asp in controls (~20 nM) and, most interestingly, an increase of ~5 times of this D-amino acid content in knock-out mice. Moreover, in agreement with previous *in vitro* studies (Davies and Johnston, 1976; Malthe-Sørenssen et al., 1979; Nakatsuka et al., 2001; Savage et al., 2001; Raiteri et al., 2007; D'Aniello et al., 2011), we found that endogenous free D-Asp is released also *in vivo* by neurons through a Ca^{2+}-dependent mechanism, as extracellular concentration of this D-amino acid is below the detection limit in Ca^{2+}-free condition. Unexpectedly, we also detected increased extracellular L-Asp levels in *Ddo* $^{-/-}$ mice but unchanged total content of the L-isomer, as reported also in other studies (Errico et al., 2006; Han et al., 2015). In the attempt to explain such an interesting result, we hypothesize that exaggerated intracellular accumulation of free D-Asp may locally alter the racemization rate of D-Asp to L-Asp in the cortical nerve terminals and/or affect the mechanism of L-Asp release and uptake. Unlike extracellular D-Asp and L-Asp, we did not find any difference in the extracellular levels of L-Glu detected in the PFC of *Ddo* $^{+/+}$ and *Ddo* $^{-/-}$ mice. However, as shown for free D-Asp, the release of both L-Asp and L-Glu was suppressed in dialysates without Ca^{2+}. Although this effect is expected for classical neurotransmitters, the *in vivo* evidence of free D-Asp clearance suggests that this D-amino acid can be actively and efficiently removed from the extracellular space, likely

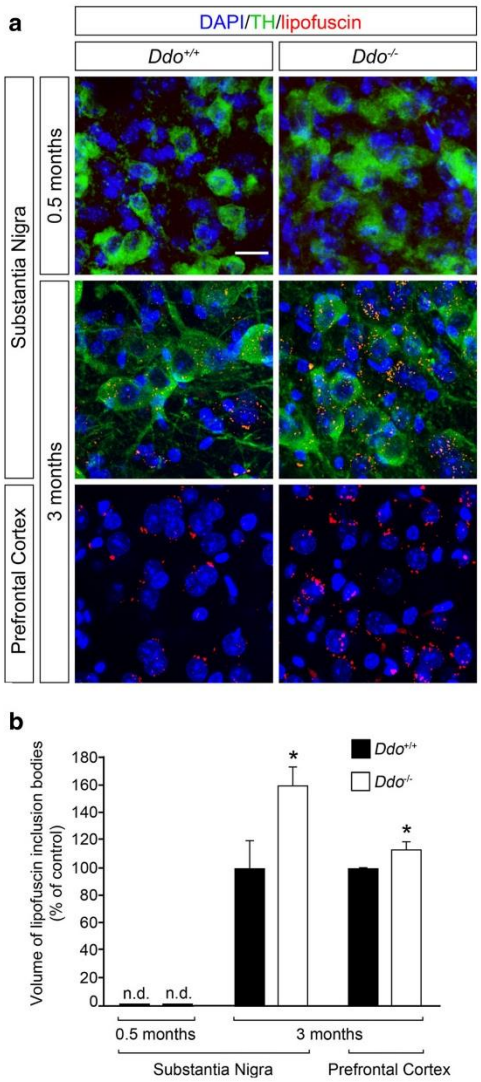

Figure 7. Increased age-dependent lipofuscin accumulation in the substantia nigra pars compacta and prefrontal cortex of *Ddo* $^{-/-}$ mice. ***a***, Representative high-magnification confocal images of the substantia nigra pars compacta and prefrontal cortex (layers V-VI) of *Ddo* $^{+/+}$ and *Ddo* $^{-/-}$ mice at 0.5 and 3 months of age ($n = 3$ per genotype and age). Higher accumulation of lipofuscin granules (red) appears evident in 3-month-old *Ddo* $^{-/-}$ compared with *Ddo* $^{+/+}$ specimens in both TH-immunostained (green) dopaminergic neurons as well as in deep layers (V-VI) of the prefrontal cortex. ***b***, Quantification of lipofuscin inclusion bodies volume in the substantia nigra and prefrontal cortex. Data are mean ± SEM. n.d., Nondetectable. $^{*}p < 0.05$, compared with *Ddo* $^{+/+}$ mice (Student's *t* test). Scale bar, 5 μm.

through L-Glu/L-Asp transport system, which has been previously shown to mediate the *in vitro* uptake of both Asp enantiomers approximately with the same affinity (Arriza et al., 1994, 1997; Palacín et al., 1998).

Despite that the existence of enzymes catalyzing the degradation of D-amino acids is long established (Krebs, 1935), the role of DDO in the brain has been puzzling because of the negligible levels of its endogenous substrates. Importantly, herein we report that DDO exerts its physiological role by protecting the brain from the neurotoxic effects induced by persistently higher extracellular levels of its substrate, D-Asp, known to act as an NMDAR agonist. Indeed, consistent with the knowledge that sustained overactivation of NMDARs at extrasynaptic sites is detrimental for neuronal survival (Lipton, 2008; Hardingham and Bading, 2010; Parsons and Raymond, 2014), we showed that the lack of DDO in knock-out mice, through the resulting persistent spillover of extracellular D-Asp, triggers precocious oxidative stress, activation of caspase-3, and cell death in the PFC and SN. Interestingly, coexpression of activated caspase-3 with NeuN in the PFC, and with TH in the SN, demonstrates that cell death in these brain areas of *Ddo* $^{-/-}$ mice involves pyramidal and dopaminergic neurons, respectively. On the other side, active caspase-3 immunoreaction is also, to some extent, detected outside NeuN- and TH-positive neurons, thus suggesting that apoptotic events triggered by increased D-Asp levels are not exclusive of these cell types.

Previous findings have demonstrated that D-Asp is the best substrate for human and mouse DDO, followed by NMDA (Setoyama and Miura, 1997; Katane et al., 2015a). Indeed, the mouse enzyme is also active on D-Glu and D-asparagine, but the relative activity is only 3.7% and 1.3% of the one determined for D-Asp (no activity was instead detected on D-histidine and other D-amino acids). Accordingly, it is conceivable that the activity of mouse DDO is too low to affect the cellular levels of these alternative substrates that, in turn, cannot contribute to the phenotypes observed in *Ddo* $^{-/-}$ mice. In addition to D-Asp, we have previously reported increased endogenous levels of NMDA in brain *Ddo* $^{-/-}$ homogenates. However, the content of NMDA in knock-out brains is hundreds-fold lower than D-Asp (Errico et al., 2006, 2011c). Therefore, we think that the contribution of this molecule to the overstimulation of NMDARs in *Ddo* $^{-/-}$ brain is likely negligible compared with that produced by the massive accumulation of free D-Asp.

Neurodegenerative events in knock-out mice are accompanied by substantial changes in microglia morphology. Indeed, we found in the SN an age-dependent phenotypic shift of microglia from hypertrophic toward a dystrophic one. This could be explained assuming that, in an early stage (3, 6 months), reactive microglia are in charge with the removal of high caspase-3-positive apoptotic cells, including clusters of lipopigments, such as lipofuscin (Riga et al., 2006), thus becoming overloaded and dystrophic in a late phase (10, 13 months). Strikingly, the observation of dystrophic microglia in a mouse model is quite a rare finding because this kind of cell does not appear with aging in rodents, as they do in humans during aging and in aging-related neurodegenerative disorders, including Alzheimer's disease (Streit and Xue, 2014; Streit et al., 2014).

Together, these data are coherent with previous morphological, functional, and *in vivo* observations indicating that constitutively upregulated levels of D-Asp in aged (6-month-old onwards) *Ddo* $^{-/-}$ mice lead to the progressive decay of synaptic transmission and plasticity, ERK signaling, cognitive abilities, and increased sensitivity to phencyclidine-induced prepulse inhibition deficit (Errico et al., 2011b; Cristino et al., 2015). Conversely, higher free D-Asp content in young-adult *Ddo* $^{-/-}$ mice has beneficial NMDAR-mediated effects because it enhances hippocampal early- and late-phase LTP (Errico et al., 2008b, 2011b,

2014), ERK phosphorylation (Errico et al., 2011b), and dendritic length and spine density (Errico et al., 2014), ameliorates spatial memory (Errico et al., 2008a, 2011b), and reduces prepulse inhibition deficits produced by psychotomimetic drugs, such as amphetamine, MK801, and phencyclidine (Errico et al., 2008a, 2015b). The opposite phenotypes shown by $Ddo^{-/-}$ mice at different phases of postnatal life highlight the peculiarity of this animal model to reproduce the dichotomous behavior of NMDAR signaling, which is able to promote synaptic plasticity and cognition or excitotoxicity depending on the subcellular localization (synaptic vs extrasynaptic activation). Further studies are needed to investigate how constitutive increase of free D-Asp can trigger synaptic or extrasynaptic NMDAR signaling in a time-dependent manner.

Notably, the abnormal precocious cell death produced by constitutively elevated free D-Asp levels in $Ddo^{-/-}$ brains suggests that DDO may control the vulnerability to neurodegeneration by hindering the endogenous accumulation of its substrate. Conversely, the physiological abundance of free D-Asp in the embryonic and perinatal brain, due to negligible *Ddo* expression and enzyme activity (Van Veldhoven et al., 1991), indicates that the physiological role of D-Asp must be restricted to a limited developmental time window, after which its high content would be harmful. In this regard, it is mandatory that the generation of conditional $Ddo^{-/-}$ mice and the employment of inhibitors for DDO enzyme (Katane et al., 2015b) to test the safety of transient D-Asp increase (as opposed to the detrimental effects of its persistent elevation) in the adult brain.

In conclusion, our results show, for the first time, that the progressive demethylation of the putative *Ddo* promoter is the mechanism for the postnatal onset and subsequent increase of *Ddo* expression that, in turn, is critical to regulate the content of the NMDAR agonist, D-Asp, in adulthood. In a mouse model with constitutively suppressed *Ddo* expression, we demonstrated that deregulated extracellular levels of D-Asp are able to produce early oxidative stress and cell death, thus unmasking a key role for DDO in counteracting precocious neurodegeneration produced by excessive NMDAR stimulation. In this light, $Ddo^{-/-}$ mice represent a novel animal model of accelerated brain aging deterioration with potential application for *in vivo* screening of anti-aging compounds.

References

Arriza JL, Fairman WA, Wadiche JI, Murdoch GH, Kavanaugh MP, Amara SG (1994) Functional comparisons of three glutamate transporter subtypes cloned from human motor cortex. J Neurosci 14:5559–5569. Medline

Arriza JL, Eliasof S, Kavanaugh MP, Amara SG (1997) Excitatory amino acid transporter 5, a retinal glutamate transporter coupled to a chloride conductance. Proc Natl Acad Sci U S A 94:4155–4160. CrossRef Medline

Bifulco D, Pollegioni L, Tessaro D, Servi S, Molla G (2013) A thermostable L-aspartate oxidase: a new tool for biotechnological applications. Appl Microbiol Biotechnol 97:7285–7295. CrossRef Medline

Brunk UT, Terman A (2002) Lipofuscin: mechanisms of age-related accumulation and influence on cell function. Free Radic Biol Med 33:611–619. CrossRef Medline

Cristino L, Luongo L, Squillace M, Paolone G, Mango D, Piccinin S, Zianni E, Imperatore R, Iannotta M, Longo F, Errico F, Vescovi AL, Morari M, Maione S, Gardoni F, Nisticò R, Usiello A (2015) D-Aspartate oxidase influences glutamatergic system homeostasis in mammalian brain. Neurobiol Aging 36:1890–1902. CrossRef Medline

D'Aniello A, Vetere A, Petrucelli L (1993) Further study on the specificity of D-amino acid oxidase and D-aspartate oxidase and time course for complete oxidation of D-amino acids. Comp Biochem Physiol 105:731–734. Medline

D'Aniello S, Somorjai I, Garcia-Fernàndez J, Topo E, D'Aniello A (2011) D-Aspartic acid is a novel endogenous neurotransmitter. FASEB J 25: 1014–1027. CrossRef Medline

Davies LP, Johnston GA (1976) Uptake and release of D-and L-aspartate by rat brain slices. J Neurochem 26:1007–1014. CrossRef Medline

Dunlop DS, Neidle A, McHale D, Dunlop DM, Lajtha A (1986) The presence of free D-aspartic acid in rodents and man. Biochem Biophys Res Commun 141:27–32. CrossRef Medline

Errico F, Pirro MT, Affuso A, Spinelli P, De Felice M, D'Aniello A, Di Lauro R (2006) A physiological mechanism to regulate D-aspartic acid and NMDA levels in mammals revealed by D-aspartate oxidase deficient mice. Gene 374:50–57. CrossRef Medline

Errico F, Rossi S, Napolitano F, Catuogno V, Topo E, Fisone G, D'Aniello A, Centonze D, Usiello A (2008a) D-Aspartate prevents corticostriatal long-term depression and attenuates schizophrenia-like symptoms induced by amphetamine and MK-801. J Neurosci 28:10404–10414. CrossRef Medline

Errico F, Nisticò R, Palma G, Federici M, Affuso A, Brilli E, Topo E, Centonze D, Bernardi G, Bozzi Y, D'Aniello A, Di Lauro R, Mercuri NB, Usiello A (2008b) Increased levels of D-aspartate in the hippocampus enhance LTP but do not facilitate cognitive flexibility. Mol Cell Neurosci 37:236–246. CrossRef Medline

Errico F, Nisticò R, Napolitano F, Mazzola C, Astone D, Pisapia T, Giustizieri M, D'Aniello A, Mercuri NB, Usiello A (2011a) Increased D-aspartate brain content rescues hippocampal age-related synaptic plasticity deterioration of mice. Neurobiol Aging 32:2229–2243. CrossRef Medline

Errico F, Nisticò R, Napolitano F, Oliva AB, Romano R, Barbieri F, Florio T, Russo C, Mercuri NB, Usiello A (2011b) Persistent increase of D-aspartate in D-aspartate oxidase mutant mice induces a precocious hippocampal age-dependent synaptic plasticity and spatial memory decay. Neurobiol Aging 32:2061–2074. CrossRef Medline

Errico F, Bonito-Oliva A, Bagetta V, Vitucci D, Romano R, Zianni E, Napolitano F, Marinucci S, Di Luca M, Calabresi P, Fisone G, Carta M, Picconi B, Gardoni F, Usiello A (2011c) Higher free D-aspartate and N-methyl-D-aspartate levels prevent striatal depotentiation and anticipate L-DOPA-induced dyskinesia. Exp Neurol 232:240–250. CrossRef Medline

Errico F, Napolitano F, Nisticò R, Usiello A (2012) New insights on the role of free D-aspartate in the mammalian brain. Amino Acids 43:1861–1871. CrossRef Medline

Errico F, Napolitano F, Squillace M, Vitucci D, Blasi G, de Bartolomeis A, Bertolino A, D'Aniello A, Usiello A (2013) Decreased levels of d-aspartate and NMDA in the prefrontal cortex and striatum of patients with schizophrenia. J Psychiatr Res 47:1432–1437. CrossRef Medline

Errico F, Nisticò R, Di Giorgio A, Squillace M, Vitucci D, Galbusera A, Piccinin S, Mango D, Fazio L, Middei S, Trizio S, Mercuri NB, Teule MA, Centonze D, Gozzi A, Blasi G, Bertolino A, Usiello A (2014) Free D-aspartate regulates neuronal dendritic morphology, synaptic plasticity, gray matter volume and brain activity in mammals. Transl Psychiatry 4:e417. CrossRef Medline

Errico F, Mothet JP, Usiello A (2015a) D-Aspartate: an endogenous NMDA receptor agonist enriched in the developing brain with potential involvement in schizophrenia. J Pharm Biomed Anal 116:7–17. CrossRef Medline

Errico F, D'Argenio V, Sforazzini F, Iasevoli F, Squillace M, Guerri G, Napolitano F, Angrisano T, Di Maio A, Keller S, Vitucci D, Galbusera A, Chiariotti L, Bertolino A, de Bartolomeis A, Salvatore F, Gozzi A, Usiello A (2015b) A role for D-aspartate oxidase in schizophrenia and in schizophrenia-related symptoms induced by phencyclidine in mice. Transl Psychiatry 5:e512. CrossRef Medline

Gavin DP, Chase KA, Sharma RP (2013) Active DNA demethylation in postmitotic neurons: a reason for optimism. Neuropharmacology 75: 233–245. CrossRef Medline

Guida F, Luongo L, Marmo F, Romano R, Iannotta M, Napolitano F, Belardo C, Marabese I, D'Aniello A, De Gregorio D, Rossi F, Piscitelli F, Lattanzi R, de Bartolomeis A, Usiello A, Di Marzo V, de Novellis V, Maione S (2015) Palmitoylethanolamide reduces pain-related behaviors and restores glutamatergic synapses homeostasis in the medial prefrontal cortex of neuropathic mice. Mol Brain 8:47. CrossRef Medline

Han H, Miyoshi Y, Koga R, Mita M, Konno R, Hamase K (2015) Changes in D-aspartic acid and D-glutamic acid levels in the tissues and physiological fluids of mice with various d-aspartate oxidase activities. J Pharm Biomed Anal 116:47–52. CrossRef Medline

Hardingham GE, Bading H (2010) Synaptic versus extrasynaptic NMDA receptor signalling: implications for neurodegenerative disorders. Nat Rev Neurosci 11:682–696. CrossRef Medline

Hashimoto A, Kumashiro S, Nishikawa T, Oka T, Takahashi K, Mito T,

Takashima S, Doi N, Mizutani Y, Yamazaki T (1993) Embryonic development and postnatal changes in free D-aspartate and D-serine in the human prefrontal cortex. J Neurochem 61:348–351. CrossRef Medline

Hashimoto A, Oka T, Nishikawa T (1995) Anatomical distribution and postnatal changes in endogenous free D-aspartate and D-serine in rat brain and periphery. Eur J Neurosci 7:1657–1663. CrossRef Medline

Heresco-Levy U, Javitt DC, Ebstein R, Vass A, Lichtenberg P, Bar G, Catinari S, Ermilov M (2005) D-Serine efficacy as add-on pharmacotherapy to risperidone and olanzapine for treatment-refractory schizophrenia. Biol Psychiatry 57:577–585. CrossRef Medline

Huang AS, Beigneux A, Weil ZM, Kim PM, Molliver ME, Blackshaw S, Nelson RJ, Young SG, Snyder SH (2006) D-Aspartate regulates melanocortin formation and function: behavioral alterations in D-aspartate oxidase-deficient mice. J Neurosci 26:2814–2819. CrossRef Medline

Kantrowitz JT, Malhotra AK, Cornblatt B, Silipo G, Balla A, Suckow RF, D'Souza C, Saksa J, Woods SW, Javitt DC (2010) High dose D-serine in the treatment of schizophrenia. Schizophr Res 121:125–130. CrossRef Medline

Katane M, Kawata T, Nakayama K, Saitoh Y, Kaneko Y, Matsuda S, Saitoh Y, Miyamoto T, Sekine M, Homma H (2015a) Characterization of the enzymatic and structural properties of human D-aspartate oxidase and comparison with those of the rat and mouse enzymes. Biol Pharm Bull 38: 298–305. CrossRef Medline

Katane M, Yamada S, Kawaguchi G, Chinen M, Matsumura M, Ando T, Doi I, Nakayama K, Kaneko Y, Matsuda S, Saitoh Y, Miyamoto T, Sekine M, Yamaotsu N, Hirono S, Homma H (2015b) Identification of novel D-aspartate oxidase inhibitors by in silico screening and their functional and structural characterization in vitro. J Med Chem 58:7328–7340. CrossRef Medline

Krashia P, Ledonne A, Nobili A, Cordella A, Errico F, Usiello A, D'Amelio M, Mercuri NB, Guatteo E, Carunchio I (2015) Persistent elevation of D-aspartate enhances NMDA receptor-mediated responses in mouse substantia nigra pars compacta dopamine neurons. Neuropharmacology 103:69–78. CrossRef Medline

Krebs HA (1935) Metabolism of amino-acids: deamination of amino-acids. Biochem J 29:1620–1644. CrossRef Medline

Lane HY, Chang YC, Liu YC, Chiu CC, Tsai GE (2005) Sarcosine or D-serine add-on treatment for acute exacerbation of schizophrenia: a randomized, double-blind, placebo-controlled study. Arch Gen Psychiatry 62:1196–1204. CrossRef Medline

Lipton SA (2008) NMDA receptor activity regulates transcription of antioxidant pathways. Nat Neurosci 11:381–382. CrossRef Medline

Malthe-Sørenssen D, Skrede KK, Fonnum F (1979) Calcium-dependent release of D-[^{3}H]aspartate evoked by selective electrical stimulation of excitatory afferent fibres to hippocampal pyramidal cells in vitro. Neuroscience 4:1255–1263. CrossRef Medline

Marutha Ravindran CR, Ticku MK (2005) Role of CpG islands in the up-regulation of NMDA receptor NR2B gene expression following chronic ethanol treatment of cultured cortical neurons of mice. Neurochem Int 46:313–327. CrossRef Medline

Migliarini S, Pacini G, Pelosi B, Lunardi G, Pasqualetti M (2013) Lack of brain serotonin affects postnatal development and serotonergic neuronal circuitry formation. Mol Psychiatry 18:1106–1118. CrossRef Medline

Nakatsuka S, Hayashi M, Muroyama A, Otsuka M, Kozaki S, Yamada H, Moriyama Y (2001) D-Aspartate is stored in secretory granules and released through a Ca(2+)-dependent pathway in a subset of rat pheochromocytoma PC12 cells. J Biol Chem 276:26589–26596. CrossRef Medline

Negri A, Tedeschi G, Ceciliani F, Ronchi S (1999) Purification of beef kidney D-aspartate oxidase overexpressed in *Escherichia coli* and characterization of its redox potentials and oxidative activity towards agonists and antagonists of excitatory amino acid receptors. Biochim Biophys Acta 1431:212–222. CrossRef Medline

Neidle A, Dunlop DS (1990) Developmental changes in free D-aspartic acid in the chicken embryo and in the neonatal rat. Life Sci 46:1517–1522. CrossRef Medline

Nelson ED, Kavalali ET, Monteggia LM (2008) Activity-dependent suppression of miniature neurotransmission through the regulation of DNA methylation. J Neurosci 28:395–406. CrossRef Medline

Palacín M, Estévez R, Bertran J, Zorzano A (1998) Molecular biology of mammalian plasma membrane amino acid transporters. Physiol Rev 78: 969–1054. Medline

Parsons MP, Raymond LA (2014) Extrasynaptic NMDA receptor involvement in central nervous system disorders. Neuron 82:279–293. CrossRef Medline

Raiteri L, Zappettini S, Milanese M, Fedele E, Raiteri M, Bonanno G (2007) Mechanisms of glutamate release elicited in rat cerebrocortical nerve endings by 'pathologically' elevated extraterminal K^+ concentrations. J Neurochem 103:952–961. CrossRef Medline

Riga D, Riga S, Halalau F, Schneider F (2006) Brain lipopigment accumulation in normal and pathological aging. Ann N Y Acad Sci 1067:158–163. CrossRef Medline

Sacchi S, Lorenzi S, Molla G, Pilone MS, Rossetti C, Pollegioni L (2002) Engineering the substrate specificity of D-amino-acid oxidase. J Biol Chem 277:27510–27516. CrossRef Medline

Sakai K, Homma H, Lee JA, Fukushima T, Santa T, Tashiro K, Iwatsubo T, Imai K (1998) Emergence of D-aspartic acid in the differentiating neurons of the rat central nervous system. Brain Res 808:65–71. CrossRef Medline

Savage DD, Galindo R, Queen SA, Paxton LL, Allan AM (2001) Characterization of electrically evoked [^{3}H]-D-aspartate release from hippocampal slices. Neurochem Int 38:255–267. CrossRef Medline

Schell MJ, Cooper OB, Snyder SH (1997) D-aspartate localizations imply neuronal and neuroendocrine roles. Proc Natl Acad Sci U S A 94:2013–2018. CrossRef Medline

Setoyama C, Miura R (1997) Structural and functional characterization of the human brain D-aspartate oxidase. J Biochem 121:798–803. CrossRef Medline

Shalini S, Dorstyn L, Dawar S, Kumar S (2015) Old, new and emerging functions of caspases. Cell Death Differ 22:526–539. CrossRef Medline

Sisalli MJ, Secondo A, Esposito A, Valsecchi V, Savoia C, Di Renzo GF, Annunziato L, Scorziello A (2014) Endoplasmic reticulum refilling and mitochondrial calcium extrusion promoted in neurons by NCX1 and NCX3 in ischemic preconditioning are determinant for neuroprotection. Cell Death Differ 21:1142–1149. CrossRef Medline

Still JL, Buell MV (1949) Studies on the cyclophorase system: D-aspartic oxidase. J Biol Chem 179:831–837. Medline

Streit WJ, Xue QS (2014) Human CNS immune senescence and neurodegeneration. Curr Opin Immunol 29:93–96. CrossRef Medline

Streit WJ, Braak H, Xue QS, Bechmann I (2009) Dystrophic (senescent) rather than activated microglial cells are associated with tau pathology and likely precede neurodegeneration in Alzheimer's disease. Acta Neuropathol 118:475–485. CrossRef Medline

Streit WJ, Xue QS, Tischer J, Bechmann I (2014) Microglial pathology. Acta Neuropathol Commun 2:142. CrossRef Medline

Topo E, Fisher G, Sorricelli A, Errico F, Usiello A, D'Aniello A (2010) Thyroid hormones and D-aspartic acid, D-aspartate oxidase, D-aspartate racemase, H_2O_2, and ROS in rats and mice. Chem Biodivers 7:1467–1478. CrossRef Medline

Tsai G, Yang P, Chung LC, Lange N, Coyle JT (1998) D-Serine added to antipsychotics for the treatment of schizophrenia. Biol Psychiatry 44: 1081–1089. CrossRef Medline

Tsai GE, Yang P, Chang YC, Chong MY (2006) D-Alanine added to antipsychotics for the treatment of schizophrenia. Biol Psychiatry 59:230–234. CrossRef Medline

Van Veldhoven PP, Brees C, Mannaerts GP (1991) D-Aspartate oxidase, a peroxisomal enzyme in liver of rat and man. Biochim Biophys Acta 1073: 203–208. CrossRef Medline

Wolosker H, D'Aniello A, Snyder SH (2000) D-Aspartate disposition in neuronal and endocrine tissues: ontogeny, biosynthesis and release. Neuroscience 100:183–189. CrossRef Medline

Zaar K, Köst HP, Schad A, Volkl A, Baumgart E, Fahimi HD (2002) Cellular and subcellular distribution of D-aspartate oxidase in human and rat brain. J Comp Neurol 450:272–282. CrossRef Medline

A Tph2GFP reporter stem cell line to model in vitro and in vivo serotonergic neuron development and function

In this article, an embryonic stem mouse (mES) cell line has been engineered in order to replace the Tph2 gene, the rate limiting-enzyme in serotonin (5HT) synthesis, with the GFP reporter by means of knock-in strategy. The selective expression of GFP upon differentiation toward the serotonergic fate allows to use this stem cell line for the study of serotonergic neurons development and function *in vitro*. I participated in the immunocytochemical and immunohistochemical characterization of mES-5HT neurons.

ACS Chemical Neuroscience

Research Article

pubs.acs.org/chemneuro

A *Tph2*^{GFP} Reporter Stem Cell Line To Model *in Vitro* and *in Vivo* Serotonergic Neuron Development and Function

Giulia Pacini,[†] Attilio Marino,[†,▽] Sara Migliarini,[†] Elisa Brilli,[†] Barbara Pelosi,[†] Giacomo Maddaloni,[†] Marta Pratelli,[†] Mario Pellegrino,[‡,§] Aldo Ferrari,[∥] and Massimo Pasqualetti*[,†,⊥,#]

[†]Department of Biology, Unit of Cell and Developmental Biology, University of Pisa, 56127 Pisa, Italy

[‡]Dipartimento di Ricerca Traslazionale e delle Nuove Tecnologie in Medicina e Chirurgia, University of Pisa, 56126 Pisa, Italy

[§]Istituto Nazionale di Ottica, National Research Council (CNR), 56124 Pisa, Italy

[∥]ETH Zurich, Laboratory of Thermodynamics in Emerging Technologies, 8092 Zurich, Switzerland

[⊥]Center for Neuroscience and Cognitive Systems, Istituto Italiano di Tecnologia, 38068 Rovereto (TN), Italy

[#]Neuroscience Institute, National Research Council (CNR), 56124 Pisa, Italy

Supporting Information

ABSTRACT: Modeling biological systems *in vitro* has contributed to clarification of complex mechanisms in simplified and controlled experimental conditions. Mouse embryonic stem (mES) cells can be successfully differentiated toward specific neuronal cell fates, thus representing an attractive tool to dissect, *in vitro*, mechanisms that underlie complex neuronal features. In this study, we generated and characterized a reporter mES cell line, called *Tph2*^{GFP}, in which the vital reporter GFP replaces the *tryptophan hydroxylase 2* (*Tph2*) gene. *Tph2*^{GFP} mES cells selectively express GFP upon *in vitro* differentiation toward the serotonergic fate, they synthesize serotonin, possess excitable membranes, and show the typical morphological, morphometrical, and molecular features of *in vivo* serotonergic neurons. Thanks to the vital reporter GFP, we highlighted by time-lapse video microscopy several dynamic processes such as cell migration and axonal outgrowth in living cultures. Finally, we demonstrated that predifferentiated *Tph2*^{GFP} cells are able to terminally differentiate, integrate, and innervate the host brain when grafted *in vivo*. On the whole, the present study introduces the *Tph2*^{GFP} mES cell line as a useful tool allowing accurate developmental and dynamic studies and representing a reliable platform for the study of serotonergic neurons in health and disease.

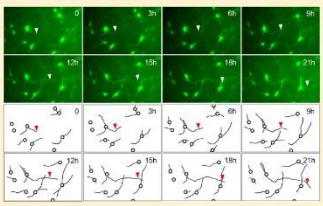

KEYWORDS: *Embryonic stem cells, 5-HT, in vitro differentiation, serotonergic neurons, vital serotonergic differentiation sensor, in vivo grafting*

INTRODUCTION

Serotonin (5-HT) is a neurotransmitter with a broad spectrum of physiological functions, ranging from the regulation of crucial events during brain development[1−3] to the modulation of emotional, affective, cognitive, and autonomic functions in adulthood.[4−11] Serotonergic neurons are clustered in 9 raphe nuclei within the brainstem and provide an extensive axonal network that covers nearly the entire central nervous system[12,13] (CNS). The synthesis of serotonin requires the catalytic activity of the tryptophan hydroxylase 2 (Tph2) enzyme that is selectively expressed in serotonergic neurons upon their differentiation.[14]

Interestingly, impairments of 5-HT neurotransmission have been associated with several neurologic disorders such as depression, anxiety, obsessive-compulsive disorder, autism, and schizophrenia, suggesting a central role for 5-HT in normal brain functioning.[15,16] Understanding the mechanisms regulating 5-HT neurotransmission in health and disease is therefore of high medical relevance, especially for the development of new therapies targeting 5-HT neurotransmission. However, the neurobiology of 5-HT neurons and the mechanisms underlying their development are only beginning to be elucidated.

In order to understand these complex phenomena, a well-standardized model system is needed. The use of *in vitro* biological systems has provided remarkable insights in the understanding of complex mechanisms involved in both development and function of specific cell types, allowing the investigators to work in simplified and controlled environments. In recent years, the efforts of distinct laboratories have focused on developing several *in vitro* models of serotonergic neurons, derived from human fibroblasts and human/mouse embryonic stem (ES) cells.[17−22]

The generation of innovative *in vitro* models allowing the investigation of dynamic processes can be easily achieved combining the use of mouse ES (mES) cells, which provide an

Special Issue: Serotonin Research 2016

Received: November 24, 2016
Accepted: December 28, 2016
Published: December 28, 2016

DOI: 10.1021/acschemneuro.6b00403
ACS Chem. Neurosci. XXXX, XXX, XXX−XXX

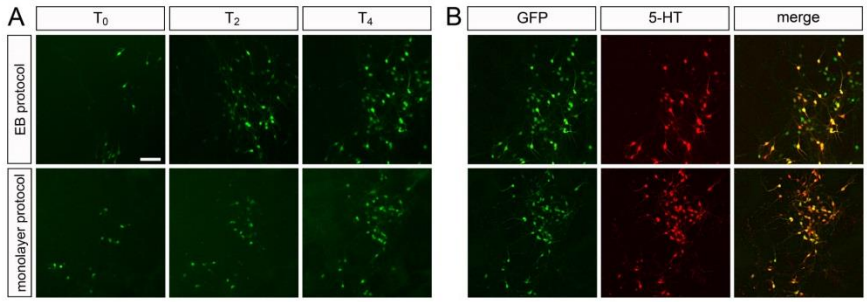

Figure 1. *Tph2*^{GFP} mES cell derived neurons differentiated with either the EB or the monolayer protocol. (A) Live GFP imaging of the same field starting from the day of appearance of the first GFP$^+$ cell (T_0) and 2 days (T_2) and 4 days (T_4) later. (B) Immunocytochemistry performed at day T_4 on the same cells showing, in the same field as in panel A, colabeling of GFP and 5-HT within *Tph2*^{GFP} mES cell derived neurons. Scale bar: 150 μm.

extraordinary source of distinct cell types through *in vitro* differentiation,[23,24] with the expression of vital fluorescent reporters.

Herein, we generated the *Tph2*^{GFP} knock-in mES cell line, in which the *Tph2* gene has been replaced by *GFP* resulting in the specific expression of the reporter in mature serotonergic neurons. Molecular, cellular, and physiological characterization of *Tph2*^{GFP} mES cell line demonstrated that this model system provides a simple and reliable *in vitro* platform to study several aspects of the development and the biology of serotonergic neurons, in both standard and challenging conditions.

■ RESULTS AND DISCUSSION

***Tph2*^{GFP} Knock-in ESCs Highlights Serotonergic Neuron Differentiation *in Vitro*.** Understanding the mechanisms underlying development, plasticity, and functions of brain serotonergic neurons is of great interest in both basic and translational research. The ability to genetically trace with a vital reporter a specific type of living cells within a heterogeneous population is highly attractive and allows the analysis of dynamic processes particularly relevant in developmental biology. Therefore, we engineered mES cells to express the vital reporter GFP in differentiated serotonergic neurons by a knock-in strategy into the Tph2 locus. Indeed, Tph2 is the most specific marker for serotonergic neurons due to two main features: (i) the timing of Tph2 expression is tightly correlated to serotonergic neuron terminal differentiation; (ii) Tph2 is selectively expressed in serotonergic neurons of the raphe system. The *Tph2*^{GFP} line was generated from the *Tph2*$^{GFP(FRT\text{-}neo\text{-}FRT)}$ knock-in mES cell line previously obtained.[3] Transient transfection of a *Flp*-expressing vector was used to remove the *neo* cassette and avoid the transcriptional repression of *GFP* expression by the FRT-flanked *neo* cassette (Supporting Information Figure S1A). A total of 59 recombinant mES cell clones in which the *neo* cassette was excised were identified by both polymerase chain reaction (PCR) and Southern blot, with 3 of them resulting to be pure recombined clones (Supporting Information Figure S1B,C). Sequencing analysis confirmed the integrity of the locus of the newly recombinant *Tph2*^{GFP} allele generated (not shown). The 3 *Tph2*^{GFP} mES cell clones retained typical parental mES cell morphology, normal karyotype (19, XY), and pluripotency, as they expressed stem cell molecular markers such as *Oct4* and showed alkaline phosphatase (AP) enzymatic activity (Supporting Information Figure S1D-E).

To test the specificity of the GFP expression in differentiated serotonergic neurons within a mixed neuronal cell population, we differentiated the *Tph2*^{GFP} mES cells using the embryoid body (EB)-based five stage protocol established by Lee and collaborators[25] (hereafter referred as EB protocol; Supporting Information Figure S2A) that promotes the differentiation of a wide variety of neuronal subtypes *in vitro*. Upon administration of specific mitogens and growth factors (i.e., FGF2, SHH, FGF8), EB protocol allowed us to obtain fluorescent cells starting from differentiation day 18 (d18; n = 12 independent experiments). GFP-positive (GFP$^+$) cells showed a neuronal-like morphology and contained extensive processes. The appearance of the first fluorescent cell was defined as T_0 (Figure 1A) and both the number of GFP$^+$ cells and the intensity of live fluorescence strongly increased over time indicating that differentiation was proceeding (Figure 1A). Double immunocytochemistry assay on the same specimens revealed that all the GFP$^+$ cells are also 5-HT$^+$ and *vice versa* (Figure 1B), although the intensity of the immunolabeling for 5-HT is variable and not tightly correlated to the intensity of the GFP signal. On the whole, these data demonstrated that GFP expression was selectively activated upon serotonergic neuron differentiation, allowing the GFP reporter to be used as a selective marker for 5-HT neurons *in vitro*.

It is worth noting that the *Tph2*^{GFP} recombinant allele brought the disruption of *Tph2* gene function, the rate-limiting enzyme in 5-HT synthesis. However, *Tph2*^{GFP}+/− mice did not show alterations in the development of 5-HT neurons and in 5-HT brain content as compared to wild-type mice, either during gestation or in adulthood, suggesting that *Tph2* heterozygosis did not affect cell phenotype.[3]

An Alternative Protocol for *Tph2*^{GFP} ESC *in Vitro* Differentiation. ES cells represent a powerful tool to perform high-throughput studies in simplified and controlled conditions. In this regard, the availability of cheaper methods for differentiating ES cells would be a great advantage, especially for scaled-up applications. Therefore, we wondered whether shorter and cost-effective protocols could be used to efficiently differentiate *Tph2*^{GFP} mES cells. As Fico and collaborators (2008) described a low confluence monolayer cell culture in Knockout Serum Replacement (KSR)-supplemented medium inducing a reliable *in vitro* neural differentiation[26] (hereafter referred as "monolayer protocol"), we used such a protocol to differentiate *Tph2*^{GFP} mES cells (Supporting Information Figure S2B). Results showed a reliable and robust neuronal differ-

DOI: 10.1021/acschemneuro.6b00403
ACS Chem. Neurosci. XXXX, XXX, XXX−XXX

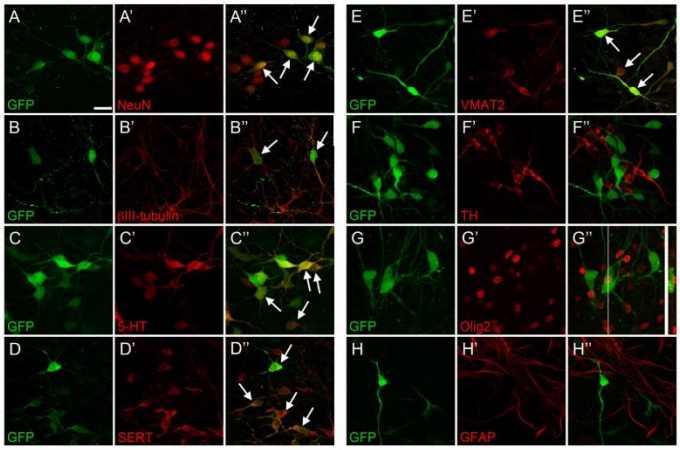

Figure 2. mES-5HT neurons show a *bona fide* serotonergic molecular identity. Representative confocal images of d13 mES-5HT neurons showing that GFP$^+$ cells express typical postmitotic neuronal markers (NeuN, A−A″; βIII-tubulin, B−B″), synthesize 5-HT (C−C″), and possess the mature serotonergic machinery (SERT, D−D″; VMAT2, E−E″). GFP expression is restricted to cells showing the 5-HTergic phenotype, as it was undetectable in dopaminergic (TH, F−F″) or astroglia cell types (Olig2, G-G″; GFAP, H−H″). Double labeled cells are highlighted by arrows. Scale bar: 20 μm.

entiation allowing us to observe GFP expression in living differentiating cell cultures (Figure 1A). The timing of appearance of GFP$^+$ cells ranged from day 7 to day 11 (n = 10 independent experiments) and colocalization of GFP and 5-HT signals was confirmed by immunocytochemistry experiments (Figure 1B). We then quantified the efficiency of serotonergic differentiation of the EB and the monolayer protocol scoring GFP-NeuN double positive cells. An efficiency of 16.6 ± 0.3% and 15.1 ± 0.1% GFP-positive serotonergic cells of the NeuN-positive neurons was achieved with the EB protocol and the monolayer protocol, respectively (Supporting Information Figure S3A,B). We next compared the nature of the differentiating cells between the two protocols by means of RT-PCR analysis. Results showed that the presence of GFP$^+$ neurons *in vitro* correlated with the activation of markers of serotonergic differentiation pathway, such as *Shh*,[27] *Nkx2.2*,[28,29] and *Lmx1b*,[29,30] and with the expression of markers specific for serotonergic lineage, such as *Tph2*,[14] *SERT*,[31−33] and *Pet1*,[29,34] independently of the protocol used (Supporting Information Figure S3C).

In recent years, several efficient protocols for mES cell differentiation toward serotonergic neurons have been set up, all requiring the use of specific differentiation/growth factors such as *noggin* or *FGF2*, *FGF4*, and *FGF8*.[18,19] Our data demonstrated that the monolayer protocol had a comparable differentiation efficiency as the EB protocol and it was quicker in achieving 5-HTergic differentiation without the requirement of expensive mitogens, making this methodology cheaper and therefore more suitable for scaled-up applications. Most importantly, the lack of intermediate steps, such as cell dissociation and replating, renders our *Tph2*^{GFP} mES cells suitable for automated manipulation and scaled-up applications. For these reasons, the results shown from now on were performed on *Tph2*^{GFP} mES cell-derived 5-HT (mES-5HT) neurons differentiated using the monolayer protocol.

Cellular and Functional Characterization of mES-5HT Neurons. To better characterize the molecular features of monolayer-derived GFP$^+$ cells, we used a panel of molecular markers specific for either serotonergic phonotype or different neuronal and glial subtypes. Fluorescence immunocytochemistry analysis performed at day 13 revealed that cells expressing GFP have exited the cell cycle as they expressed neuronal postmitotic markers such as NeuN, βIII-tubulin, and Map2 (Figure 2A−A″, B−B″, and not shown). Most importantly, GFP$^+$ neurons synthesized the neurotransmitter serotonin (Figure 2C−C″) and they expressed SERT and VMAT2 (Figure 2D−D″, E−E″), two key proteins for serotonergic neuronal functionality.[33,35] SERT immunofluorescence was detected also in GFP$^-$ cells (Figure 2D−D″) according to the fact that during neurodevelopment such transporter is not selectively expressed in serotonergic neurons.[36] Besides, we did not detect any GFP$^+$ cell positive for TH, Olig2, GFAP, or Ng2 (Figure 2F−F″, G−G″, H−H″, and not shown). These results proved that GFP expression is specifically restricted to 5-HTergic lineage and showed that the monolayer protocol allowed us to differentiate a heterogeneous neuronal-glial cell population whose characteristics resemble the *in vivo* features of the developing hindbrain (e.g., SERT expression by non-serotonergic neurons; presence of serotonergic and dopaminergic neurons and glial cells).

We then investigated the functionality of mES-5HT neurons with several approaches. First, we stained for synaptophisin (Syp), a marker of synaptic structure. Syp labeling observed in GFP$^+$ mES-5HT neurons resembled that of *in vivo* GFP$^+$ fibers, thus suggesting the presence of *in vitro* neurotransmission-competent membranes (Supporting Information Figure S4). Subsequently, we used confocal calcium imaging and patch clamp recordings to better characterize the functionality of mES-5HT neurons. In order to visualize calcium influx, we loaded GFP$^+$ neurons with a calcium sensitive dye, Fluo4-AM. In the absence of depolarizing stimuli, we detected a weak

DOI: 10.1021/acschemneuro.6b00403
ACS Chem. Neurosci. XXXX, XXX, XXX−XXX

calcium signal, while 50 mM KCl depolarizing stimulus induced a strong increase in fluorescence emission (Supporting Information Figure S5, Supporting Information movie 1), suggesting that mES-5HT neurons have voltage-gated calcium channels. Moreover, we investigated the presence of voltage-gated sodium channels, whose expression is an essential hallmark of neuronal excitability. To this aim, we stimulated mES-5HT neurons with veratridine, an activator of voltage-gated sodium channels,[37] which is able to induce calcium transients in mature neurons.[38] Our results showed that 20 μM veratridine induced a remarkable increase of the Ca^{2+} signal in GFP^+ cells (n = 15; Figure 3A–D). No calcium transients were detected by treating neurons with vehicle or stimulating undifferentiated mES cells with 20 μM veratridine. These results demonstrated the presence of functional voltage-gated sodium and calcium channels in GFP^+ neurons.

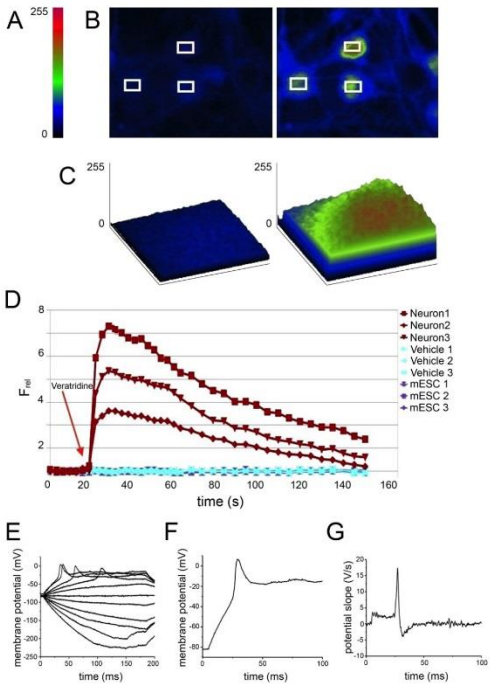

Figure 3. Characterization of functional properties of GFP^+ mES-5HT neurons. (A–D) Intracellular calcium influx was detected in GFP^+ neurons after application of veratridine stimulus. (A) Pseudocolor calibration bar. (B) Representative fluorescence time lapse images before (left) and after (right) veratridine stimulus (3 regions of interest are outlined in white). (C) Fluorescence intensity surface plot of a region of interest before (left) and after (right) the veratridine stimulus. (D) Time course of the F_{rel} (red, GFP^+ mES-5HT neurons stimulated with veratridine; light-blue, GFP^+ mES-5HT neurons stimulated with vehicle; violet, mES cells stimulated with veratridine). (E–G) Electrophysiological recordings of GFP^+ mES-5HT neurons with patch clamp technique. (E) Typical superposed whole-cell membrane potential traces induced by applying hyperpolarizing and depolarizing currents (in the range between −50 and +50 pA) from a holding potential of −80 mV. (F) Voltage response displaying the shorter latency and (G) the slope of membrane potential.

Patch clamp recordings were performed in current clamp on GFP^+ mES-5HT neurons after 14–21 days of differentiation. The resting membrane potential was −34.7 ± 3.6 mV (n = 22). Depolarizing currents induced in about 75% of the recorded neurons a spike-like response (Figure 3E–G), indicating the development of membrane electrical excitability, in keeping with the results obtained with calcium imaging. Patch clamp recordings together with results from confocal calcium imaging showed the presence and the proper functionality of voltage-gated ion channels on GFP^+ mES-5HT neurons, demonstrating the excitability of neuron membranes.

Overall, the presence of synaptophisin and KCl- and veratridine-mediated intracellular Ca^{2+} response, together with patch clamp recordings, suggested the development of a functional membrane in *in vitro* differentiated 5-HT neurons.

Morphological Characterization of mES-5HT Neurons. Traditional descriptive studies have highlighted the heterogeneity of serotonergic neurons in terms of different cell body size, morphology, and dendrite orientation.[39] To verify if our *in vitro* model could recapitulate those *in vivo* observations, we performed a comparative analysis between GFP^+ mES-5HT neurons and GFP^+ 5-HT neurons in the raphe of $Tph2^{GFP}$ heterozygous mice. Results highlighted that mES-5HT neurons showed either bipolar or multipolar shape with a broad spectrum of cell body dimension, resembling those present *in vivo* (Figure 4A). We then performed a morphometric study on GFP^+ mES-5HT neurons to compare the size of neuronal somas to those of *in vivo* GFP^+ 5-HT neurons. To achieve optimal staining of GFP^+ cell soma, both *in vivo* and *in vitro* samples were immunostained with an anti-GFP antibody. Results demonstrated that the soma size range of mES-5HT neurons closely matched that observed in *in vivo* 5-HT neurons, with the only exception that larger-cell-body subtypes were under-represented *in vitro* as compared to *in vivo* samples (Figure 4B). To date, the broad heterogeneity of serotonergic neurons in cell morphology, electrophysiological property, and molecular profile have been extensively proved.[39−41] This difference seems to be related to both developmental origins and anatomical position within the raphe nuclei. Our data suggest that *in vitro* differentiated 5-HT neurons recapitulate, from a morphological and morphometrical point of view, the complexity of 5-HTergic system. On these bases, it is tempting to speculate that $Tph2^{GFP}$ mES cells are capable to give rise to all serotonergic neuron subpopulations. For this reason, it will be of interest to determine whether mES-5HT neurons could recapitulate also the heterogeneity of serotonergic neurons in terms of gene-expression profile and electrophysiological property. If so, our *in vitro* system could potentially be used as a valuable tool to analyze how and when the heterogeneity of serotonergic neurons occurs during development.

***Tph2*^{GFP} mES Cells As a Tool to Highlight *in Vitro* Dynamic Processes of Serotonin Neurons Development and Differentiation.** The specific expression in 5-HT neurons of a fluorescent vital reporter allows the analysis of dynamic events, critical in neuronal development and function. To visualize the genesis and behavior of mature serotonergic neurons, we performed time-lapse recordings on *in vitro* $Tph2^{GFP}$ cells starting from differentiation day 10. GFP live fluorescence in mature 5-HT neurons allowed us to analyze the appearance of differentiated neurons (Supporting Information Figure S6A, Supporting Information movie 2) and their

DOI: 10.1021/acschemneuro.6b00403
ACS Chem. Neurosci. XXXX, XXX, XXX−XXX

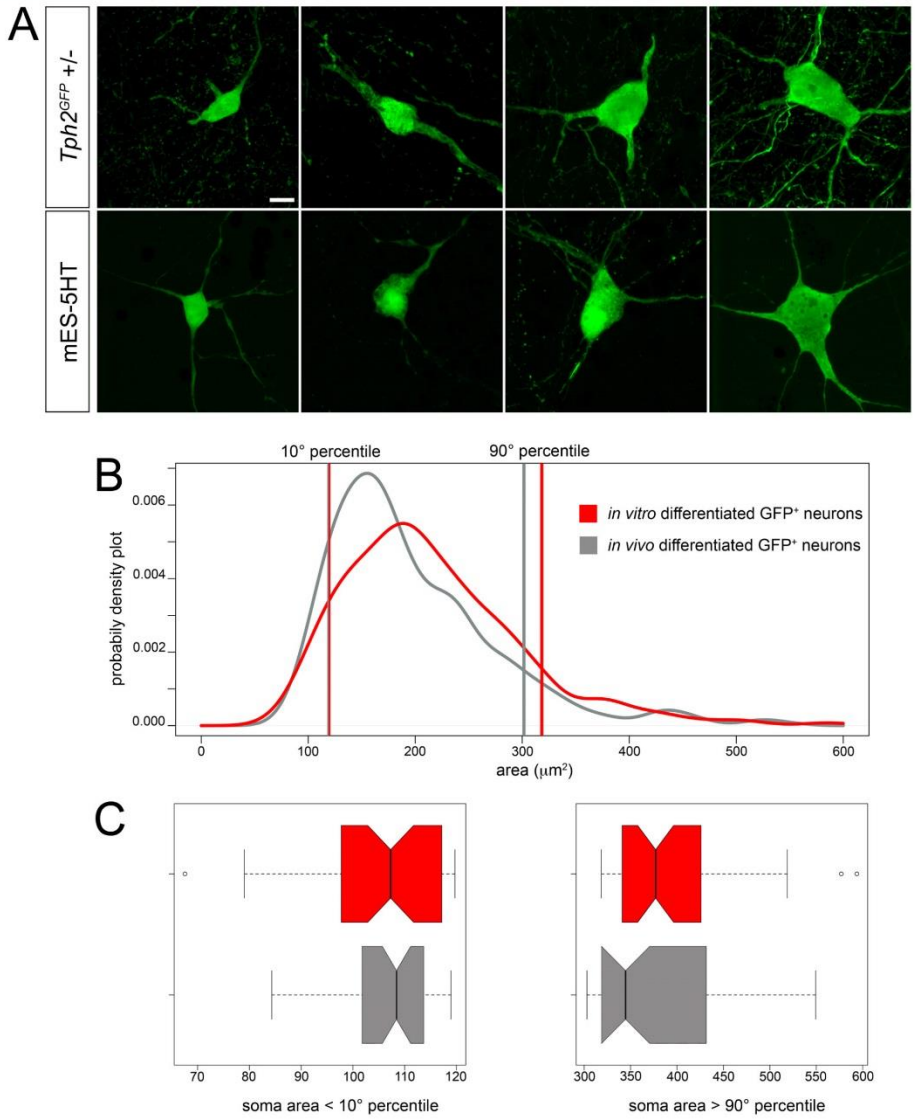

Figure 4. mES-5HT neurons display the morphological and morphometric features typical of *in vivo* serotonergic neurons. (A) Representative confocal images comparing the size and the shape of the cell soma of *in vivo* serotonergic neurons (top row) with those of mES-5HT neurons (bottom row). (B) Probability density functions showing the distribution of the soma areas of *in vivo* serotonergic neurons (gray; $n = 469$) and of mES-5HT neurons (red; $n = 480$). (C) Box plots comparing the tails of the probability distribution of the soma areas between *in vivo* 5-HT neurons (gray; $n = 47$) and mES-5HT neurons (red; $n = 48$). Scale bar: 10 μm.

motility, highlighting both changes in morphology and process elongation/retraction (Supporting Information Figure S6B, Supporting Information movie 3). We observed in mES-5HT neurons the extension of a leading process and movement of the cell body and nucleus (nucleokinesis; Figure 5, Supporting Information movie 4). The cell body of mES-5HT neurons acquired a bipolar shape thanks to a leading process (Figure 5B–D), ahead of the soma, that started to undergo rapid movements of both elongation and retraction. Subsequently, the leading process stabilized, and we observed both the retraction of the trailing process and a forward movement of the soma into the leading process (Figure 5E–H, Supporting

DOI: 10.1021/acschemneuro.6b00403
ACS Chem. Neurosci. XXXX, XXX, XXX−XXX

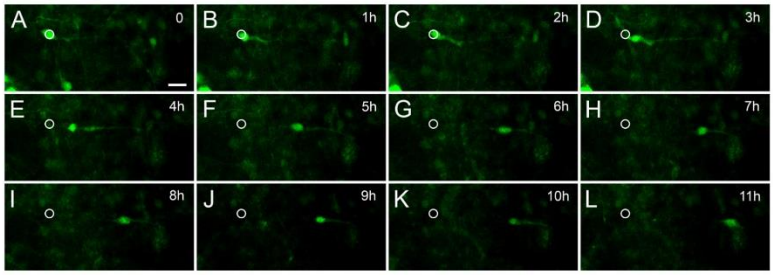

Figure 5. Cell migration of mES cell-derived 5-HT neurons. (A–L) Representative 4D wide-field fluorescent microscopy images acquired every hour showing the nucleokinetic migration of *in vitro* differentiated 5-HT neurons. Circle marks the original position of the cell soma, and the arrowhead indicates the progression of the cell body along the leading neurite. Scale bar: 15 μm.

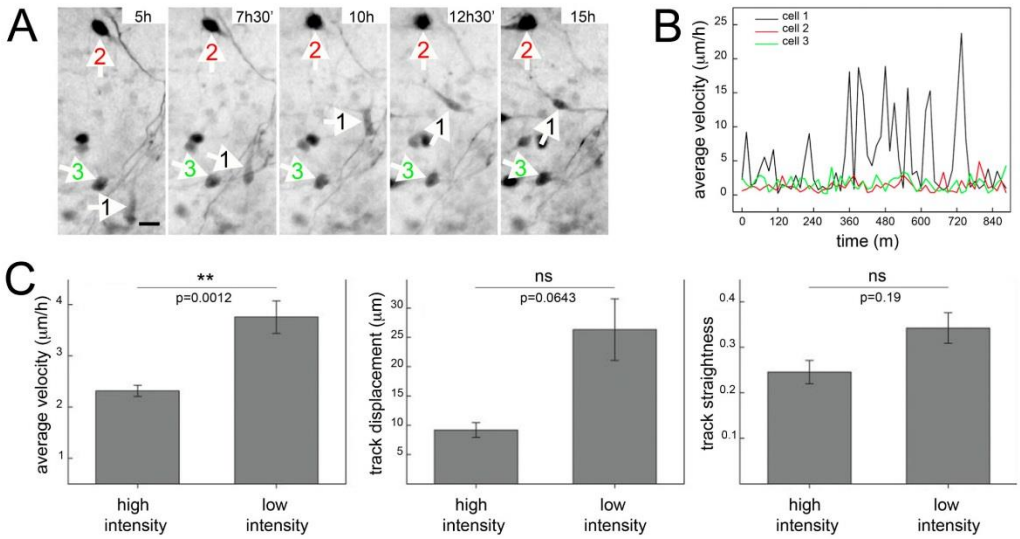

Figure 6. Analysis of mES-5HT neuron migratory velocity. (A) Representative 4D fluorescent wide-field microscopy images of mES-5HT neurons acquired in the same field every 150 min. At each time point, arrows track the position of three cells with a different intensity of GFP fluorescence. (B) Graph showing the average velocity for each of the three cells highlighted in panel A measured at different time points (ΔT = 20 min) over 840 min. (C) Graphs comparing the average velocity, the track displacement, and the track straightness (ratio between the total length of the track and the Euclidian distance between the starting point and the final point), between mES-5HT neurons with either high or low GFP intensity (n = 93; ns, nonsignificant). Scale bar: 10 μm.

Information movie 4). Thanks to time-lapse recordings, we noted that mES-5HT neurons showed distinct motility properties as well as different GFP fluorescence levels (Figure 6). As fluorescence intensity increased over time after terminal differentiation likely due to GFP accumulation within cells, we therefore investigated a possible correlation between GFP fluorescence level and neuronal motility by 4D fluorescent microscopy track recordings of individual mES-5HT neurons. Results showed that GFP signal was negatively correlated to neuronal displacement velocity. The mean speed of neurons with low GFP signal was significantly higher than that of neurons expressing high GFP level ($p < 0.01$, Figure 6C).

Our *in vitro* model recapitulates some characteristics described *in vivo* such as the nucleokinetic migration of postmitotic serotonergic precursors during their movement along the dorso-ventral axis to form the raphe nuclei.[42] As GFP accumulation over time in mES-5HT neurons after differentiation parallels the progressive decline of their migratory capacity, these *in vitro* findings may recapitulate what is likely occurring *in vivo* when 5-HT neurons moving toward their final target location progressively reduce their migratory potential and eventually stop migrating.

In Vivo Transplantation of *Tph2*^{GFP} Neural Precursors.

Cell transplantation into a specific tissue or organ of animal models is an important biological paradigm for studying cellular phenotypes in a physiological context.[43−45] To understand how *Tph2*^{GFP} mES cell-derived serotonergic neurons behave *in vivo*, we performed grafting experiments in postnatal mouse brain. *Tph2*^{GFP} mES cells were allowed to differentiate for 7 days using the monolayer protocol to obtain a population enriched

DOI: 10.1021/acschemneuro.6b00403
ACS Chem. Neurosci. XXXX, XXX, XXX−XXX

in neuronal precursor cells,[26] then dissociated, and grafted into the raphe region of CD1 pups at postnatal day 2 (n = 18). Cells were observed under the fluorescent microscope before grafting to assess the absence of GFP expression. Grafts were analyzed at different time points after transplantation (1, 10, and 25 weeks) by GFP and 5-HT immunofluorescence. After transplantation in the host mouse brain, $Tph2^{GFP}$ neural precursors survived and differentiated toward the serotonergic phenotype as highlighted by the presence of GFP$^+$ neurons immunoreactive for 5-HT as early as 1 week post transplantation (Figure 7). Importantly, GFP$^+$ grafted cells acquired the typical

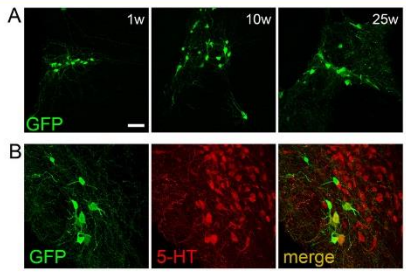

Figure 7. $Tph2^{GFP}$ neural precursors express GFP and produce 5-HT upon *in vivo* transplantation. (A) Representative confocal images showing the presence of GFP immunolabeled neurons in sagittal brain sections of mice transplanted with $Tph2^{GFP}$ neural precursors 1 (1w), 10 (10w) and 25 (25w) weeks after injection. (B) Confocal images of brain sagittal sections of 25w transplanted mice immunostained for 5-HT and GFP. Scale bar: 50 μm (A); 20 μm (B).

morphology of mature serotonergic neurons, which was maintained over time as shown by the presence of mES-5HT neurons in the host brain at 25 weeks postgrafting (n = 4; Figure 7). GFP$^+$ neurons developed extensive fibers innervating distal targets in the host brain and showing axon varicosities, a morphological landmark of mature 5-HT neurons (Supporting Information Figure S7). We did not observe teratoma formation after grafting,[46,47] suggesting that 7 days of predifferentiating treatment smothered the capacity of $Tph2^{GFP}$ cells to induce tumors.

On the whole, the survival and the differentiation toward the serotonergic lineage of $Tph2^{GFP}$ neural precursors as well as the capability of mES-5HT neurons to innervate the host brain suggested that grafted serotonergic neurons likely integrate into host neuronal circuits.

■ CONCLUSIONS

The generation of appropriate *in vitro* models allowing the study of complex processes in a simplified and controlled environment could provide remarkable insights into the functional role of serotonin. Here, we have generated and characterized the $Tph2^{GFP}$ mES cell line, which can be used as *in vitro* sensor for 5-HT neuron differentiation. We showed that mES-5HT neurons specifically express GFP, synthesize 5-HT, and exhibit excitable membranes. The presence of a vital reporter made $Tph2^{GFP}$ mES cell-derived 5-HT neurons particularly suitable for dynamic studies, such as cell differentiation, migration, and axonal outgrowth, both *in vitro* and *in vivo* upon grafts in host brains. In conclusion, $Tph2^{GFP}$ mES cell line represents a novel tool allowing dissection of the mechanisms underlying 5-HT neuron development and function, in a simplified and controlled manner.

■ METHODS

Generation of $Tph2^{GFP}$ Mouse Embryonic Stem Cell Line. $Tph2^{GFP(FRT\text{-}neo\text{-}FRT)}$ knock-in allele was previously generated using the mES cell line E14Tg2a.4.[3] $Tph2^{GFP(FRT\text{-}neo\text{-}FRT)}$ cells were electroporated with *pCAGGS-FLPe* vector[48] and maintained for 48 h in 1 μg/mL puromycin selection, to allow the transient expression of the *Flp* recombinase. Clones were screened for the recombination event by polymerase chain reaction (PCR) using the following primer sets: forward 5′-GTAGGTGTCATTCTATTCTGGG-3′; reverse 5′-GATAGGGAACTTCACTTTCTATTT-3′. For Southern blot analysis *Hin*dIII digests were hybridized with a probe designed on *Tph2* exon I. The expected size for the *Tph2* wild-type, $Tph2^{GFP(FRT\text{-}neo\text{-}FRT)}$, and $Tph2^{GFP}$ alleles were 0.8 kb, 3.6 kb, and 1.6 kb, respectively.

Alkaline Phosphatase Activity Assay. Cells were fixed in 4% paraformaldeyde in PBS and rinsed twice in PBS. Cells were than incubated in NBT/BCIP (20 μL/mL) up to 5 min. The reaction was stopped by rinsing samples with PBS.

mES Cell Culture Maintenance. Undifferentiated $Tph2^{GFP}$ mES cells were routinely maintained on gelatin-coated dishes in mES cell medium containing Glasgow minimum essential medium (GMEM, Sigma-Aldrich) supplemented with 10% fetal bovine serum (FBS, EU Approved Euromed, Euroclone), 2 mM L-glutamine (Life Technologies), 0.1 mM nonessential amino acids (Life Technologies), 1 mM sodium pyruvate (Life Technologies), 0.05 mM β-mercaptoethanol (Sigma-Aldrich), antibiotics, and 10^3 units/mL Leukemia inhibitory factor (LIF, Millipore).

Neural Differentiation. *EB Protocol.* mES cells were differentiated following the protocol described by Lee and collaborators,[25] modified as follows. Embryoid bodies (EBs) were generated on nonadherent dishes for 3 days in mES cell medium in the absence of LIF (EB medium). EBs were then plated onto gelatin coated tissue culture dishes in the same medium. After 24 h, selection of neural precursor cells was initiated, replacing the medium with serum-free ITSFn medium.[49] After 6−8 days of selection, cells were dissociated and seeded on polyornithine (15 mg/mL; Sigma) and fibronectin (1 mg/mL; Sigma) coated dishes or glass coverslip. Expansion of neural precursors were allowed in N2 (ITS Technologies) supplemented medium with 1 μg/mL laminin (Sigma-Aldrich) in the presence of 20 ng/mL FGF2 (R&D Systems), 500 ng/mL Shh-N (R&D Systems), and 100 ng/mL FGF8 (R&D Systems), 2 mM L-glutamine (Life Technologies), 0.08 mM β-mercaptoethanol (Sigma-Aldrich), and antibiotics. After 3−6 days expansion, differentiation was induced by changing the medium with serum free N2 (ITS Technologies) supplemented medium with 1 μg/mL laminin (Sigma-Aldrich). Cells were incubated under differentiation conditions for 7−15 days.

Monolayer Protocol. Monolayer protocol for neural differentiation was performed following ref 26 with minor modifications. Briefly, undifferentiated mES cells were dissociated in single-cell suspension, and 1500−3000 cells/cm^2 were seeded on gelatin-coated plates or coverslips. Differentiating cell culture was maintained in KnockOut DMEM (Life Technologies) supplemented with 15% KnockOut Serum Replacement (KSR, Life Tecnologies), 2 mM L-glutamine (Life Technologies), 0.1 mM β-mercaptoethanol (Sigma-Aldrich), and antibiotics.

RT-PCR. Total RNA was prepared using Nucleospin RNA-XS total RNA purification kit (Macherey-Nagel). For cDNA synthesis, random hexamer primers (Promega) were used to prime reverse transcriptase (RT) reactions. The cDNA synthesis was carried out using ImProm-II Reverse Transcriptase (Promega) following the manufacturer's instructions. To analyze relative expression of different mRNAs, the amount of cDNA was normalized based on the signal from ubiquitously expressed β-actin mRNA. Level of neural mRNAs present in ES cell culture was compared to that in undifferentiated ES cells. PCR was carried out using standard protocols with GoTaq polymerase (Promega). Primer sequence (forward and reverse) was as follows: β-actin, For 5′-AGGCATCACTATTGGCAACGA-3′, Rev 5′-

DOI: 10.1021/acschemneuro.6b00403
ACS Chem. Neurosci. XXXX, XXX, XXX−XXX

CCGATCCACACAGAGTACTTG-3′; *Oct3/4*, For 5′-ATTTGC-CAAGCTCCTGAAGCAG-3′, Rev 5′-TTGATCGCTTGCCCT-TCTGG-3′; *Tph2*, For 5′-CAGTTCCTCCTTCATCTCTGC-3′, Rev 5′-CGCTTTTCTTGTCCTCGC-3′; *SERT*, For 5′-CCTGCA-GATCCATCAGTCAA-3′, Rev 5′-TGTAAGGGAAGGTGGCTGTC-3′; *Tph1*, For 5′-CATTAGAAGTATGTCCACGGGC-3′, Rev 5′-ACTCTCCCTCTTTCGGAGGA-3′ *Shh*, For 5′-GGAAGATCA-CAAGAAACTCCGAAC-3′, Rev 5′-GGATGCGAGCTTTGGATT-CATAG-3′; *Nkx 2.2*, For 5′-ATGTCGCTGACCAACACAAA-3′, Rev 5′-AAAGGGCTCTTAAGGGGCAG-3′; *Lmx1b*, For 5′-CCTCAG-CGTGCGTGTGGTC-3′, Rev 5′-AGCAGTCGCTGAGGCTGGTG-3′; *Pet1*, For 5′-ATGAGACAGAGCGGCACCT-3′, Rev 5′-CCA-GGAGAAACTGCCACAAC-3′; *TH*, For 5′-AGGGATGGGAAT-GCTGTTCTCA-3′, Rev 5′-ACCAGGTGGTGACACTTGTCCAA-3′; *GAD67*, For 5′-TACGGGGTTCGCACAGGTC-3′, Rev 5′-CCCCAAGCAGCATCCACAT-3′; *GFAP*, For 5′-GCGCTCAAT-GCTGGCTTCAA-3′, Rev 5′-ACGCAGCCAGGTTGTTCTCT-3′; *Olig2*, For 5′-GGCGGTGGCTTCAAGTCATC-3′, Rev 5′-TAGTTT-CGCGCCAGCAGCAG-3′.

Southern Blot. mES recombinant clones were expanded according to BayGenomics online protocols. Total genomic DNA was extracted from each clone with phenol−chloroform and ethanol precipitation, digested with specific restriction enzymes, separated according to size by gel electrophoresis, transferred to nylon filters, and hybridized with a proper radiolabeled probe. To screen for the Flp mediated recombination mES cell DNA was digested with *Hin*dIII, and a probe designed on the Tph2 exon I was used. The size of the *Tph2* wild-type, of the $Tph2^{GFP(frt\text{-}neo\text{-}frt)}$ allele, and of the $Tph2^{GFP}$ allele were 0.8 kb, 3.6 kb, and 1.6 kb, respectively.

Animals. Animals were maintained on artificial 12/12h light/dark cycle at constant temperature of 22 ± 1 °C and were housed in standard Plexiglas cages with food and water *ad libitum*. All experimental protocols were conducted in accordance with the Ethic Committee of the University of Pisa and approved by the Veterinary Department of the Italian Ministry of Health.

Immunocytochemistry and Immunohistochemistry. Immunocytochemistry was performed on cells fixed with 4% (PFA) for 15 min at RT, rinsed twice in PBS, and blocked in PBS containing 5% heat-inactivated lamb serum. Cells were incubated in primary antibody solution o/n at 4 °C. Antibodies and dilutions were as follows: chicken anti-eGFP (Aves Laboratories) 1:500; rabbit anti-eGFP (Invitrogen) 1:1000; rabbit anti-5-HT (Sigma) 1:500; mouse anti-NeuN (Chemicon) 1:100; rabbit anti-SERT (Millipore) 1:1000; mouse anti-βIII-tubulin (Millipore) 1:500; chicken anti-GFAP (Covance) 1:100; mouse anti-TH (Millipore) 1:400; chicken anti-synaptophysin1 (SYSY) 1:100; chicken anti-VMAT2 (Millipore) 1:1000; rabbit anti-Olig2 (Chemicon) 1:500. Secondary antibody dilutions were as follows: Rhodamine Red-X goat anti-rabbit IgG (Invitrogen) 1:500; fluorescein (FITC) labeled anti-chicken IgY (Aves Laboratories) 1:200. After rinse with PBS, cells were coverslipped.

For animal samples, mice were intracardially perfused using 4% PFA; brains were dissected and postfixed in PFA at 4 °C o/n. After fixation, brains were rinsed in PBS and embedded in agarose 2.5% and cut with vibratome. For immunostaining, sections are incubated with primary antibodies in PBS containing 5% heat-inactivated lamb serum and 0.1−0.5% Triton X-100, o/n at 4 °C. Primary antibody dilutions were as follows: rabbit anti-5-HT (Sigma) 1:500; chicken anti-eGFP (Aves Laboratories) 1:500. Samples were washed with PBS and 0.1−0.5% Triton X-100 and then incubated with secondary antibodies. Secondary antibody dilutions were as follows: Rhodamine Red-X goat anti-rabbit IgG (Invitrogen) 1:500; fluorescein (FITC) labeled anti-chicken IgY (Aves Laboratories) 1:200. After rinsing with PBS, cell nuclei were counterstained with DAPI and coverslipped.

Images of immunolabeled samples were performed using either an Eclipse-Ti (Nikon) or a Nikon-A1 confocal microscope. For colocalization analysis we used the "Coloc" function of the Imaris Bitplane software (version 7.2.3).

Calcium Imaging. mES-5HT neurons were cultured on gelatin-coated *IBIDI* μ-slide plates (Martinsried, Germany), and calcium imaging was performed as follows: Neurons were stained with 5 μM Ca^{2+}-sensitive membrane permeable fluorescent dye Fluo-4 AM (Invitrogen) for 20 min at RT in artificial cerebrospinal fluid (aCSF). After loading, samples were rinsed with the aCSF solution containing 10 mM 4-(2-hydroxyethyl)-1-piperazine ethanesulfonic acid (HEPES), 140 mM NaCl, 10 mM glucose, 5 mM KCl, 2 mM $CaCl_2$, 2 mM $MgCl_2$, at pH 7.4. The intracellular fluorescence level was monitored using a confocal laser scanning microscope (Biorad, Radiance Plus) equipped with a 40× objective (NA 1.3; Nikon). After an equilibration period of 30 min, cells were stimulated with either 50 mM KCl isotonic solution or 25 μM veratridine (Sigma-Aldrich). Treatments were repeated three times yielding comparable results. Negative and positive controls were performed using vehicles and ionomycin, respectively. Time-lapse images were recorded every 3 s. Images were analyzed using NIH ImageJ software (http://rsb.info.nih.gov/ij/). After background subtraction, fluorescence intensity was expressed as a relative value ($F_{rel} = F_{(t)}/F_i$, where F_i is the fluorescence intensity before the stimulus and $F_{(t)}$ is the fluorescence intensity at a specific time point t).

Electrophysiological Recordings. Cell cleaning was performed by incubation for 5 min in aCSF solution containing NaCl 140 mM, KCl 5 mM, $CaCl_2$ 2 mM, $MgCl_2$ 2 mM, glucose 10 mM, Hepes 10 mM, pH 7.4, with 1 mg/mL Pronase (Calbiochem) and subsequent rinse in aCSF. Cells exhibiting fluorescence emission at 530 nm when excited at 480 nm (GFP^+) were selected for recordings that were carried out in Leibovitz 15 culture medium, supplemented with 2% fetal calf serum and 10 mM glucose. Patch-clamp was performed in whole cell current-clamp configuration. Micropipettes were pulled in two stages from 1.7/1.1 mm (outer/inner diameter) glass capillaries Blaubrand 7087 and filled with a solution containing KCl 120 mM, $CaCl_2$ 0.0001 mM, Hepes 10 mM, pH 7.4. Electrical resistance was 4−5 MΩ. A patch amplifier Heka EPC 7 was used to record the membrane potential at rest and during the application of hyperpolarizing and depolarizing currents, starting from a membrane potential held at −80 mV. The protocol of stimulation and acquisition was controlled by pClamp software (Axon) connected to a Labmaster DMA with a TL-1 interface. Data were filtered at 3 kHz and acquired at 10 kHz. Data were finally processed using Origin software.

Cell Size Measurement. Cell size measurement analysis of GFP^+ mES-5HT neurons and *in vivo* 5-HT neurons was performed using the "annotation measurement algorithm" of Nikon NIS-Elements software. For *in vivo* studies, neurons were sampled on 4 distinct parasagittal brain sections obtained from $Tph2^{GFP}$ heterozygous animals (n = 3). Probability density function graphs were obtained using Kernel density estimation. The Wilcoxon sum rank test was used to compare the tails of the distribution functions.

Time-Lapse Fluorescence Imaging and Cell Tracking. Time-lapse recordings were performed using an inverted fluorescence Eclipse-Ti (Nikon) with a perfect focus system in a chamber kept at 37 °C. Chamber stage was buffered with 5% CO_2 and maintained in a humid environment. Four dimension (4D) wide-field fluorescent microscopy images were acquired every 10 to 15 min up to a maximum of 30 h. Image postprocessing included a deconvolution step performed using Huygens Essential (Scientific Volume Imaging, The Netherlands). Tracking of the cell soma and of the neurites was performed using Imaris (Bitplane, Switzerland). Statistical comparison of population means was performed using a nonparametric Mann−Whitney U test ($\alpha = 0.05$). All quantitative measurements reported are expressed as average values ± the standard error of the mean.

Transplantation of Neural Precursors. The monolayer protocol was used to differentiate $Tph2^{GFP}$ mES cells. After 7 days, neural precursors were cultured for additional 24 h in serum free N2 (ITS Technologies) supplemented medium with 1 μg/mL laminin (Sigma-Aldrich). Cells were then dissociated, pelleted, and resuspended in ice cold PBS at a final density of 2.5×10^5 cells/μL. P2 wild type CD1 mouse pups were anesthesized on ice, and 1 μL of the cell suspension was injected unilaterally with a Hamilton syringe in the rostral hindbrain where the dorsal raphe region is located. Grafted animals were sacrificed after 1, 10, and 25 weeks after transplantation and processed for immunohistochemistry.

DOI: 10.1021/acschemneuro.6b00403
ACS Chem. Neurosci. XXXX, XXX, XXX−XXX

■ ASSOCIATED CONTENT

Supporting Information

The Supporting Information is available free of charge on the ACS Publications website at DOI: 10.1021/acschemneuro.6b00403.

Data showing the generation, differentiation, molecular and functional characteristics of the *Tph2*^{GFP} mES cells, as well as their properties upon differentiation in serotonergic neurons assessed by means of time-lapse microscopy and *in vivo* grafting (PDF)

Intracellular calcium influx in mES-5HT neurons (AVI)

Appearance of GFP signal in a mES-5HT neuron (MPG)

Neurite elongation in a GFP$^+$ mES-5HT neuron (MPG)

Nucleokinetic migration of an *in vitro* differentiated GFP$^+$ mES-5HT neuron (MPG)

■ AUTHOR INFORMATION

Corresponding Author

*Massimo Pasqualetti. Mailing address: Department of Biology, Unit of Cell and Developmental Biology, University of Pisa, SS 12 Abetone e Brennero, 56127 Pisa, Italy. Phone: +39 0502211496. E-mail: massimo.pasqualetti@unipi.it.

ORCID

Massimo Pasqualetti: 0000-0002-0844-8139

Present Address

[V]A.M.: Center for Micro-BioRobotics, Istituto Italiano di Tecnologia, 56025 Pontedera (PI), Italy.

Author Contributions

Pacini, Marino, and Pasqualetti designed research. Pacini, Marino, Migliarini, Brilli, Pelosi, Maddaloni, Pratelli, Pellegrino, Ferrari, and Pasqualetti conducted experiments and performed data analysis. Pacini and Pasqualetti wrote the manuscript.

Funding

This work was supported by Italian Ministry of Education, University and Research (MIUR) (Prin 2008, 200894SYW2), Toscana Life Sciences Foundation (Orphan_0108 program), and Norvegian Research Council to M. Pasqualetti. G.P., B.P., G.M. and M. Pratelli were supported by Ph.D. program from University of Pisa. S.M. was supported by Regional Program and European Social Fund.

Notes

The authors declare no competing financial interest.

■ ACKNOWLEDGMENTS

The authors thank Angelo De Muro for helpful suggestions. We acknowledge Cinzia Valente for excellent technical assistance and members of our laboratory for valuable discussions and comments on the manuscript.

■ REFERENCES

(1) Gaspar, P., Cases, O., and Maroteaux, L. (2003) The developmental role of serotonin: news from mouse molecular genetics. *Nat. Rev. Neurosci. 4*, 1002−1012.

(2) Daubert, E. A., and Condron, B. G. (2010) Serotonin: a regulator of neuronal morphology and circuitry. *Trends Neurosci. 33*, 424−434.

(3) Migliarini, S., Pacini, G., Pelosi, B., Lunardi, G., and Pasqualetti, M. (2013) Lack of brain serotonin affects postnatal development and serotonergic neuronal circuitry formation. *Mol. Psychiatry 18*, 1106−1118.

(4) Hendricks, T. J., Fyodorov, D. V., Wegman, L. J., Lelutiu, N. B., Pehek, E. A., Yamamoto, B., Silver, J., Weeber, E. J., Sweatt, J. D., and Deneris, E. S. (2003) Pet-1 ETS gene plays a critical role in 5-HT neuron development and is required for normal anxiety-like and aggressive behavior. *Neuron 37*, 233−247.

(5) Ruhe, H. G., Mason, N. S., and Schene, A. H. (2007) Mood is indirectly related to serotonin, norepinephrine and dopamine levels in humans: a meta-analysis of monoamine depletion studies. *Mol. Psychiatry 12*, 331−359.

(6) Lane, H. Y., Liu, Y. C., Huang, C. L., Hsieh, C. L., Chang, Y. L., Chang, L., Chang, Y. C., and Chang, W. H. (2008) Prefrontal executive function and D1, D3, 5-HT2A and 5-HT6 receptor gene variations in healthy adults. *Journal of psychiatry & neuroscience: JPN 33*, 47−53.

(7) Alenina, N., Kikic, D., Todiras, M., Mosienko, V., Qadri, F., Plehm, R., Boye, P., Vilianovitch, L., Sohr, R., Tenner, K., Hortnagl, H., and Bader, M. (2009) Growth retardation and altered autonomic control in mice lacking brain serotonin. *Proc. Natl. Acad. Sci. U. S. A. 106*, 10332−10337.

(8) Lesch, K. P., and Waider, J. (2012) Serotonin in the modulation of neural plasticity and networks: implications for neurodevelopmental disorders. *Neuron 76*, 175−191.

(9) Asan, E., Steinke, M., and Lesch, K. P. (2013) Serotonergic innervation of the amygdala: targets, receptors, and implications for stress and anxiety. *Histochem. Cell Biol. 139*, 785−813.

(10) Whitney, M. S., Shemery, A. M., et al. (2016) Adult Brain Serotonin Deficiency Causes Hyperactivity, Circadian Disruption, and Elimination of Siestas. *J. Neurosci. 36*, 9828−9842.

(11) Fernandez, S. P., Muzerelle, A., Scotto-Lomassese, S., Barik, J., Gruart, A., Delgado-Garcia, J. M., and Gaspar, P. (2017) Constitutive and Acquired Serotonin Deficiency Alters Memory and Hippocampal Synaptic Plasticity. *Neuropsychopharmacology 42*, 512.

(12) Lidov, H. G., and Molliver, M. E. (1982) Immunohistochemical study of the development of serotonergic neurons in the rat CNS. *Brain Res. Bull. 9*, 559−604.

(13) Wallace, J. A., and Lauder, J. M. (1983) Development of the serotonergic system in the rat embryo: an immunocytochemical study. *Brain Res. Bull. 10*, 459−479.

(14) Walther, D. J., Peter, J. U., Bashammakh, S., Hortnagl, H., Voits, M., Fink, H., and Bader, M. (2003) Synthesis of serotonin by a second tryptophan hydroxylase isoform. *Science (Washington, DC, U. S.) 299*, 76.

(15) Jacobs, B. L., and Müller, C. P. (2010) Handbook of the behavioral neurobiology of serotonin, in *Handbook of behavioral neuroscience*, 1st ed., Vol. 18, online resource (xv, 818 pp), Academic Press, London.

(16) Mosienko, V., Beis, D., Pasqualetti, M., Waider, J., Matthes, S., Qadri, F., Bader, M., and Alenina, N. (2015) Life without brain serotonin: reevaluation of serotonin function with mice deficient in brain serotonin synthesis. *Behav. Brain Res. 277*, 78−88.

(17) Kumar, M., Kaushalya, S. K., Gressens, P., Maiti, S., and Mani, S. (2009) Optimized derivation and functional characterization of 5-HT neurons from human embryonic stem cells. *Stem Cells Dev. 18*, 615−627.

(18) Shimada, T., Takai, Y., Shinohara, K., Yamasaki, A., Tominaga-Yoshino, K., Ogura, A., Toi, A., Asano, K., Shintani, N., Hayata-Takano, A., Baba, A., and Hashimoto, H. (2012) A simplified method to generate serotonergic neurons from mouse embryonic stem and induced pluripotent stem cells. *J. Neurochem. 122*, 81−93.

(19) Nefzger, C. M., Haynes, J. M., and Pouton, C. W. (2011) Directed expression of Gata2, Mash1, and Foxa2 synergize to induce the serotonergic neuron phenotype during in vitro differentiation of embryonic stem cells. *Stem Cells (Durham, NC, U. S.) 29*, 928−939.

(20) Nistor, G., Siegenthaler, M. M., Poirier, S. N., Rossi, S., Poole, A. J., Charlton, M. E., McNeish, J. D., Airriess, C. N., and Keirstead, H. S. (2011) Derivation of high purity neuronal progenitors from human embryonic stem cells. *PLoS One 6*, e20692.

(21) Lu, J., Zhong, X., Liu, H., Hao, L., Huang, C. T., Sherafat, M. A., Jones, J., Ayala, M., Li, L., and Zhang, S. C. (2016) Generation of serotonin neurons from human pluripotent stem cells. *Nat. Biotechnol. 34*, 89−94.

DOI: 10.1021/acschemneuro.6b00403
ACS Chem. Neurosci. XXXX, XXX, XXX−XXX

(22) Vadodaria, K. C., Mertens, J., Paquola, A., Bardy, C., Li, X., Jappelli, R., Fung, L., Marchetto, M. C., Hamm, M., Gorris, M., Koch, P., and Gage, F. H. (2016) Generation of functional human serotonergic neurons from fibroblasts. *Mol. Psychiatry 21*, 49−61.
(23) Keller, G. (2005) Embryonic stem cell differentiation: emergence of a new era in biology and medicine. *Genes Dev. 19*, 1129−1155.
(24) Murry, C. E., and Keller, G. (2008) Differentiation of embryonic stem cells to clinically relevant populations: lessons from embryonic development. *Cell 132*, 661−680.
(25) Lee, S. H., Lumelsky, N., Studer, L., Auerbach, J. M., and McKay, R. D. (2000) Efficient generation of midbrain and hindbrain neurons from mouse embryonic stem cells. *Nat. Biotechnol. 18*, 675−679.
(26) Fico, A., Manganelli, G., Simeone, M., Guido, S., Minchiotti, G., and Filosa, S. (2008) High-throughput screening-compatible single-step protocol to differentiate embryonic stem cells in neurons. *Stem Cells Dev. 17*, 573−584.
(27) Ye, W., Shimamura, K., Rubenstein, J. L., Hynes, M. A., and Rosenthal, A. (1998) FGF and Shh signals control dopaminergic and serotonergic cell fate in the anterior neural plate. *Cell 93*, 755−766.
(28) Briscoe, J., Sussel, L., Serup, P., Hartigan-O'Connor, D., Jessell, T. M., Rubenstein, J. L., and Ericson, J. (1999) Homeobox gene Nkx2.2 and specification of neuronal identity by graded Sonic hedgehog signalling. *Nature 398*, 622−627.
(29) Cheng, L., Chen, C. L., Luo, P., Tan, M., Qiu, M., Johnson, R., and Ma, Q. (2003) Lmx1b, Pet-1, and Nkx2.2 coordinately specify serotonergic neurotransmitter phenotype. *Journal of neuroscience 23*, 9961−9967.
(30) Ding, Y. Q., Marklund, U., Yuan, W., Yin, J., Wegman, L., Ericson, J., Deneris, E., Johnson, R. L., and Chen, Z. F. (2003) Lmx1b is essential for the development of serotonergic neurons. *Nat. Neurosci. 6*, 933−938.
(31) Hansson, S. R., Mezey, E., and Hoffman, B. J. (1998) Serotonin transporter messenger RNA in the developing rat brain: early expression in serotonergic neurons and transient expression in non-serotonergic neurons. *Neuroscience 83*, 1185−1201.
(32) Rattray, M., Michael, G. J., Lee, J., Wotherspoon, G., Bendotti, C., and Priestley, J. V. (1999) Intraregional variation in expression of serotonin transporter messenger RNA by 5-hydroxytryptamine neurons. *Neuroscience 88*, 169−183.
(33) Murphy, D. L., Lerner, A., Rudnick, G., and Lesch, K. P. (2004) Serotonin transporter: gene, genetic disorders, and pharmacogenetics. *Mol. Interventions 4*, 109−123.
(34) Hendricks, T., Francis, N., Fyodorov, D., and Deneris, E. S. (1999) The ETS domain factor Pet-1 is an early and precise marker of central serotonin neurons and interacts with a conserved element in serotonergic genes. *Journal of neuroscience 19*, 10348−10356.
(35) Erickson, J. D., Schafer, M. K., Bonner, T. I., Eiden, L. E., and Weihe, E. (1996) Distinct pharmacological properties and distribution in neurons and endocrine cells of two isoforms of the human vesicular monoamine transporter. *Proc. Natl. Acad. Sci. U. S. A. 93*, 5166−5171.
(36) Narboux-Neme, N., Pavone, L. M., Avallone, L., Zhuang, X., and Gaspar, P. (2008) Serotonin transporter transgenic (SERTcre) mouse line reveals developmental targets of serotonin specific reuptake inhibitors (SSRIs). *Neuropharmacology 55*, 994−1005.
(37) Levi, G., Gallo, V., and Raiteri, M. (1980) A reevaluation of veratridine as a tool for studying the depolarization-induced release of neurotransmitters from nerve endings. *Neurochem. Res. 5*, 281−295.
(38) Salvati, P., Maj, R., Caccia, C., Cervini, M. A., Fornaretto, M. G., Lamberti, E., Pevarello, P., Skeen, G. A., White, H. S., Wolf, H. H., Faravelli, L., Mazzanti, M., Mancinelli, E., Varasi, M., and Fariello, R. G. (1999) Biochemical and electrophysiological studies on the mechanism of action of PNU-151774E, a novel antiepileptic compound. *Journal of pharmacology and experimental therapeutics 288*, 1151−1159.
(39) Tork, I. (1990) Anatomy of the serotonergic system. *Ann. N. Y. Acad. Sci. 600*, 9−34, () 34−35 discussion.
(40) Okaty, B. W., Freret, M. E., Rood, B. D., Brust, R. D., Hennessy, M. L., deBairos, D., Kim, J. C., Cook, M. N., and Dymecki, S. M. (2015) Multi-Scale Molecular Deconstruction of the Serotonin Neuron System. *Neuron 88*, 774−791.
(41) Fernandez, S. P., Cauli, B., Cabezas, C., Muzerelle, A., Poncer, J. C., and Gaspar, P. (2016) Multiscale single-cell analysis reveals unique phenotypes of raphe 5-HT neurons projecting to the forebrain. *Brain Struct. Funct. 221*, 4007.
(42) Hawthorne, A. L., Wylie, C. J., Landmesser, L. T., Deneris, E. S., and Silver, J. (2010) Serotonergic neurons migrate radially through the neuroepithelium by dynamin-mediated somal translocation. *J. Neurosci. 30*, 420−430.
(43) Brustle, O., Spiro, A. C., Karram, K., Choudhary, K., Okabe, S., and McKay, R. D. (1997) In vitro-generated neural precursors participate in mammalian brain development. *Proc. Natl. Acad. Sci. U. S. A. 94*, 14809−14814.
(44) Ideguchi, M., Palmer, T. D., Recht, L. D., and Weimann, J. M. (2010) Murine embryonic stem cell-derived pyramidal neurons integrate into the cerebral cortex and appropriately project axons to subcortical targets. *J. Neurosci. 30*, 894−904.
(45) Falkner, S., Grade, S., Dimou, L., Conzelmann, K. K., Bonhoeffer, T., Gotz, M., and Hubener, M. (2016) Transplanted embryonic neurons integrate into adult neocortical circuits. *Nature 539*, 248−253.
(46) Arnhold, S., Klein, H., Semkova, I., Addicks, K., and Schraermeyer, U. (2004) Neurally selected embryonic stem cells induce tumor formation after long-term survival following engraftment into the subretinal space. *Invest. Ophthalmol. Visual Sci. 45*, 4251−4255.
(47) Thinyane, K., Baier, P. C., Schindehutte, J., Mansouri, A., Paulus, W., Trenkwalder, C., Flugge, G., and Fuchs, E. (2005) Fate of pre-differentiated mouse embryonic stem cells transplanted in unilaterally 6-hydroxydopamine lesioned rats: histological characterization of the grafted cells. *Brain Res. 1045*, 80−87.
(48) Schaft, J., Ashery-Padan, R., van der Hoeven, F., Gruss, P., and Stewart, A. F. (2001) Efficient FLP recombination in mouse ES cells and oocytes. *Genesis 31*, 6−10.
(49) Okabe, S., Forsberg-Nilsson, K., Spiro, A. C., Segal, M., and McKay, R. D. (1996) Development of neuronal precursor cells and functional postmitotic neurons from embryonic stem cells in vitro. *Mech. Dev. 59*, 89−102.

DOI: 10.1021/acschemneuro.6b00403
ACS Chem. Neurosci. XXXX, XXX, XXX−XXX